

Push-out and composite beam tests
of shear connectors

by

David Joseph Dedic

A Thesis Submitted to the
Graduate Faculty in Partial Fulfillment of the
Requirements for the Degree of
MASTER OF SCIENCE

Department: Civil Engineering

Major: Structural Engineering

Signatures have been redacted for privacy

Iowa State University
Ames, Iowa

1983

TABLE OF CONTENTS

	Page
1. INTRODUCTION	1
1.1 General	1
1.2 Objectives	3
1.3 Literature Review	4
1.4 General Test Program	6
1.4.1 Push-Out Test Program	6
1.4.2 Composite Beam Test Program	6
2. DESCRIPTION OF TEST SPECIMENS	8
2.1 Push-Out Tests	8
2.1.1 Description of Specimens	8
2.1.2 Fabrication of Specimens	17
2.1.2.1 Type A Specimens	17
2.1.2.2 Type B Specimens	19
2.1.3 Loading Apparatus and Instrumentation	22
2.2 Composite Beam Tests	24
2.2.1 Description of Specimens	26
2.2.2 Loading Apparatus and Instrumentation	34
3. TESTS AND TEST PROCEDURES	41
3.1 Push-Out Tests	41
3.2 Composite Beam Tests	42
3.2.1 Elastic Range	44
3.2.2 Ultimate Strength	45
4. TEST RESULTS AND ANALYSIS	46
4.1 Push-Out Test Results and Analysis	46
4.1.1 Type A Specimens	47
4.1.2 Type B Specimens	56

4.2	Composite Beam Test Results and Analysis	61
4.2.1	Elastic Range Test Results and Analysis	62
4.2.2	Ultimate Strength Test Results and Analysis	66
5.	SUMMARY AND CONCLUSIONS	82
5.1	Summary	82
5.2	Conclusions	85
6.	ACKNOWLEDGMENTS	86
7.	REFERENCES	87
8.	APPENDIX. LOAD-SLIP AND LOAD-SEPARATION CURVES	89

LIST OF TABLES

	Page
Table 1. Summary of push-out specimens tested	15
Table 2. Actual widths for each composite beam tested	29
Table 3. Physical properties of concrete	32
Table 4. Physical properties of steel	32
Table 5. Total number of DCDTs, deflection dials, and strain gages on each composite beam	38
Table 6. Summary of tests performed on the composite beam specimens	43
Table 7. Push-out tests: summary of test results and predicted ultimate loads for Type A specimens	49
Table 8. Description of type of failures occurring in push-out test specimens	50
Table 9. Push-out tests: summary of test results and predicted ultimate loads for Type B specimens	57
Table 10. Summary of ultimate strength test results for the composite beam specimens	63

LIST OF FIGURES

	Page
Figure 1. Details and dimensions of the push-out specimens	9
Figure 2. Angle-plus-bar shear connector (Series 1 and 3)	10
Figure 3. Channel shear connector (Series 2 and 4)	11
Figure 4. Stud shear connector (Series 5)	12
Figure 5. Double-nutted high-strength bolt shear connector (Series 6)	13
Figure 6. Epoxied high-strength bolt shear connector (Series 7)	14
Figure 7. Formwork used for constructing the push-out specimens	18
Figure 8. Location of instrumentation used in the push-out tests	23
Figure 9. Photographs of push-out specimens in place for testing	25
Figure 10. Cross-section of model bridge showing the location of longitudinal cuts	27
Figure 11. Location of composite beam sections where measure- ments of slab width and thickness were determined	28
Figure 12. Location of high-strength bolt shear connectors added to Beams #3 and #4	33
Figure 13. Photographs of composite beam test set-up showing test frame and specimen in place	35
Figure 14. Loading apparatus employed for testing the composite beams	36
Figure 15. Location of instrumentation on Beams #2 and #3	39

Figure 16.	Location of instrumentation on Beams #1 and #4	40
Figure 17.	Comparison of load-slip curves for half-scale connectors	52
Figure 18.	Comparison of load-slip curves for full-scale connectors, Type A specimens	55
Figure 19.	Comparison of load-slip curves for Series 5, 6, and 7 specimens	59
Figure 20.	Interior beam load-deflection curves for Tests A, B, and C	65
Figure 21.	Exterior beam load-deflection curves for Tests A, B, and C	65
Figure 22.	Photograph of Beam #1 showing bending of the level post-tensioning rod at the bracket	67
Figure 23.	Photographs showing concrete compressive failure in Beam #3	70
Figure 24.	Photographs of the failure mechanism in Beam #4	72
Figure 25.	Load-midspan strain curves for composite beams	74
Figure 26.	Midspan strain profiles at various values of load per point	76
Figure 27.	Comparison of theoretical and experimental load-deflection curves	77
Figure 28.	Load-end slip curves	78
Figure 29.	Load-slip curves for each composite beam	80

Figure A.1.	Load-slip curves for individual Series 1 push-out specimens	90
Figure A.2.	Load-slip curves for individual Series 2 push-out specimens	91
Figure A.3.	Load-slip curves for individual Series 3 push-out specimens	92
Figure A.4.	Load-slip curves for individual Series 4 push-out specimens	93
Figure A.5.	Load-slip curves for individual Series 5 push-out specimens	94
Figure A.6.	Load-slip curves for individual Series 6 push-out specimens	95
Figure A.7.	Load-slip curves for individual Series 7 push-out specimens	96
Figure A.8.	Representative load-separation curves for Series 1 push-out specimens	97
Figure A.9.	Representative load-separation curves for Series 2 push-out specimens	98
Figure A.10.	Representative load-separation curves for Series 3 push-out specimens	99
Figure A.11.	Representative load-separation curves for Series 4 push-out specimens	100
Figure A.12.	Representative load-separation curves for Series 5 push-out specimens	101

Figure A.13.	Representative load-separation curves for Series 6 push-out specimens	102
Figure A.14.	Representative load-separation curves for Series 7 push-out specimens	103

1. INTRODUCTION

1.1 General

After a useful life of more than 20 years, many bridges in Iowa don't comply with current bridge standards. Increases in the allowable live loads, changes in the AASHTO design and rating specifications, and the necessity to provide additional load capacity to support resurfacing for additional life have rendered these bridges inadequate. Therefore, strengthening or posting of load limits is essential.

The feasibility of strengthening bridges, in particular, single span, composite concrete slab/steel beam bridges, was considered in a study (11) conducted several years ago by the Engineering Research Institute of Iowa State University. The study, henceforth referred to as Phase I, considered the use of post-tensioning to strengthen bridges, therefore increasing the life of the bridge. A half-scale model bridge was tested and analytical procedures were utilized in order to determine the bridge's behavior when subjected to post-tensioning and vertical forces. Post-tensioning forces were applied to the steel bridge beams through brackets bolted to the bottom flanges of the beams. Findings of Phase I included recommendations to investigate the shear capacity of a post-tensioned bridge and to continue experimentation on the half-scale bridge model constructed and tested during Phase I.

A literature search revealed that only minimal data existed on the angle-plus-bar shear connectors. To obtain data on the angle-plus-

bar, as well as channels, studs, and high-strength bolts utilized as shear connectors, several push-out specimens were fabricated and tested. Additional shear connector information was obtained by sawing the bridge model from Phase I into four composite concrete slab/steel beam specimens. As the type of steel may be unknown on some of the bridges requiring strengthening, it was decided the addition of shear connectors, as well as the post-tensioning brackets, in the field should be by bolting rather than welding. Shear connectors (high-strength bolts) were added to two of the composite beam specimens before testing, while the remaining two specimens were tested "as fabricated," with only the original angle-plus-bar shear connectors.

All testing performed on the push-out and composite beam specimens consisted of static loads because fatigue wasn't considered a factor in the rehabilitation of bridges. It was concluded that a large portion of the existing bridge components' fatigue life had already been used. Results obtained from the push-out specimens were used in the composite beam tests and later in the analysis of the field bridges. The effect shear connectors had on the behavior and ultimate strength of post-tensioned composite beams was found by varying the number of shear connectors in companion specimens.

1.2 Objectives

The present research is part of an ongoing research project on the strengthening of composite, single span steel I-beam/concrete deck bridges by post-tensioning. Constructed between 1940 and 1960, these bridges were found to be inadequate in terms of shear capacity because of changes in design philosophy and methodology. Also, it was desired to check the behavior of the shear connectors in a post-tensioned composite beam.

The overall objective of this research study is to explore the behavior and ultimate strength of various shear connectors used in composite bridges. Although the results reported, herein, are limited as to the number of specimens, they should provide an indication of the actual behavior of shear connectors. The specific objectives of this study are to:

Relate appropriate AASHTO criteria to the actual behavior as determined from tests on the push-out and composite beam specimens.

Determine the behavior and capacity of the angle-plus-bar shear connector.

Develop and test high-strength bolt shear connectors.

Determine the behavior and capacity of post-tensioned, composite beam specimens before and after increasing the specimen's shear capacity.

In order to verify experimental results from the push-out specimens, as well as to develop design methodology, experimental results were

checked against predictions from AASHTO bridge specifications.

1.3 Literature Review

Numerous types of mechanical shear connectors have been proposed since the early 1920s for steel-concrete, composite construction. Although spirals, channels, and studs found wide acceptance in the United States then, stud connectors are almost exclusively used today because of their ease of installation and low cost.

The use of two slab push-out tests for the evaluation of shear connector behavior was common (17,19,21). These early investigations suggested that the strength of shear connectors obtained from push-out tests was lower than that obtained from beam tests. It was later concluded by Slutter and Driscoll (18) that this relationship was true. Also, the push-out test is still considered to be the most reliable and useful method of determining load-slip and ultimate load capacities of different types of connectors used in beams (2,13).

The use of high-strength bolts (ASTM A325) as shear connectors has been tested in a couple of situations (3,4,5). Dallam (3,4), in 1968 and 1970, reported the testing of two slab push-out and composite beam specimens with high-strength bolts (ASTM A325, various diameters) as shear connectors. The bolts were loosely attached to the steel beam section and held in place by wire-spring chairs. After the slab concrete was cured for 28 days, the bolts were tightened to the minimum specified bolt tension; the specimens were then tested to failure. It was found that the bolts exhibited a greater useful capacity and

ultimate strength than comparable studs. In 1976, Dorton et al. (5) described the use of high-strength bolts (ASTM A325, Type 3 weathering steel, 7/8 in. diameter) in push-out specimens and a full-scale test bridge. Double-nutted to the beam flange of a steel bridge stringer (H-pile section substituted in the push-out specimens), the bolts were placed in oversized holes to accommodate movement of the concrete deck, due to post-tensioning. Both the push-out specimens and the test bridge were subjected to fatigue and static loading. Dorton concluded that a high-strength bolt, in this particular configuration, could be safely used to replace a welded stud of the same diameter. In these previous studies, the bolts were placed before the concrete slab was cast.

Slutter and Driscoll (18) tested a series of composite beams and push-out specimens. They also re-evaluated the test results from other investigations in order to substantiate their conclusions. Tests were performed on composite beams with varying numbers of shear connectors. A number of different shear connectors (channels, spirals, bent studs, headed studs) were tested in the composite beam and push-out specimens. Test results from this, and previous investigations, were compared utilizing a method of analysis for determining the ultimate moment capacity of beams when a weaker shear connection than that proposed for design exists. Slutter and Driscoll concluded that the ultimate flexural capacity of a beam could be evaluated even if the number of shear connectors was less than that required to develop the theoretical ultimate bending capacity. The analysis showed that the

load-deflection curve of a beam was not significantly affected by slip if there were enough shear connectors provided to develop the theoretical ultimate bending capacity.

1.4 General Test Program

As previously stated, the research program conducted consisted of the testing of both push-out specimens and composite beam specimens. The following sections present brief descriptions of the particular specimens tested; the test programs implemented are presented in detail in later sections.

1.4.1 Push-Out Test Program

Twenty-two push-out specimens were fabricated and tested to failure. Five types of shear connectors were investigated for ultimate strength, separation behavior, and load-slip behavior. The breakdown as to type and number of specimens is as follows: 6 angle-plus-bar specimens, 5 channel specimens, 3 stud specimens, 4 epoxied high-strength bolt specimens, and 4 double-nutted high-strength bolt specimens. Relative slip and separation between the concrete and steel were measured with mechanical displacement dial gages. Load was applied using a 400 kip universal testing machine.

1.4.2 Composite Beam Test Program

The model bridge, tested in Phase I, was sawed into four composite concrete slab/steel beam specimens. Two of the specimens, one interior-type and one exterior-type, were strengthened with additional

shear connectors before testing, while the remaining two specimens were tested in the "as fabricated" condition. The loading condition for all tests consisted of two equal concentrated loads located about the span centerline so that a region of constant moment existed. Each specimen was tested several times with different levels of post-tensioning before being loaded to failure. Electrical resistance strain gages, utilized in Phase I, were used to measure strain at different locations on the specimens. Vertical deflection of the specimens, as well as relative slip between the steel beam and concrete slab, was measured with mechanical displacement dial gages.

2. DESCRIPTION OF TEST SPECIMENS

2.1 Push-Out Tests

2.1.1 Description of Specimens

The push-out specimens consisted of two sizes: one full-scale and the other half-scale. Dimensions of the specimens are shown in Figure 1. As is shown, each specimen consisted of a wide flange beam 2 ft. long with concrete slabs attached to each flange of the beam. The size of the wide flange beams utilized (W10x22 in the half-scale specimens and W10x68 in the full-scale specimens) was chosen on the basis of flange thickness of the beam sections. The flange thickness of the full-scale specimens closely approximated that of the exterior beams in existing bridges; the flange thickness in the half-scale specimens nearly equalled that of the exterior beams in the model bridge. As shown in Figures 2 and 6, and also described in Table 1, shear connectors were rigidly attached to the beam flanges by bolting or welding. Load was applied to the upper portion of the beam and transmitted into the slabs through the shear connectors. Thus, both the slabs and beam were subjected to compression.

The push-out specimens were grouped into two categories: Type A specimens (shown in Figures 2, 3, and 4) employed welded connectors installed before the concrete was poured. Type B specimens (Figures 5 and 6) had high-strength bolts inserted and tightened after the slabs had hardened and cured. Thus, Type A specimens modeled shear connectors

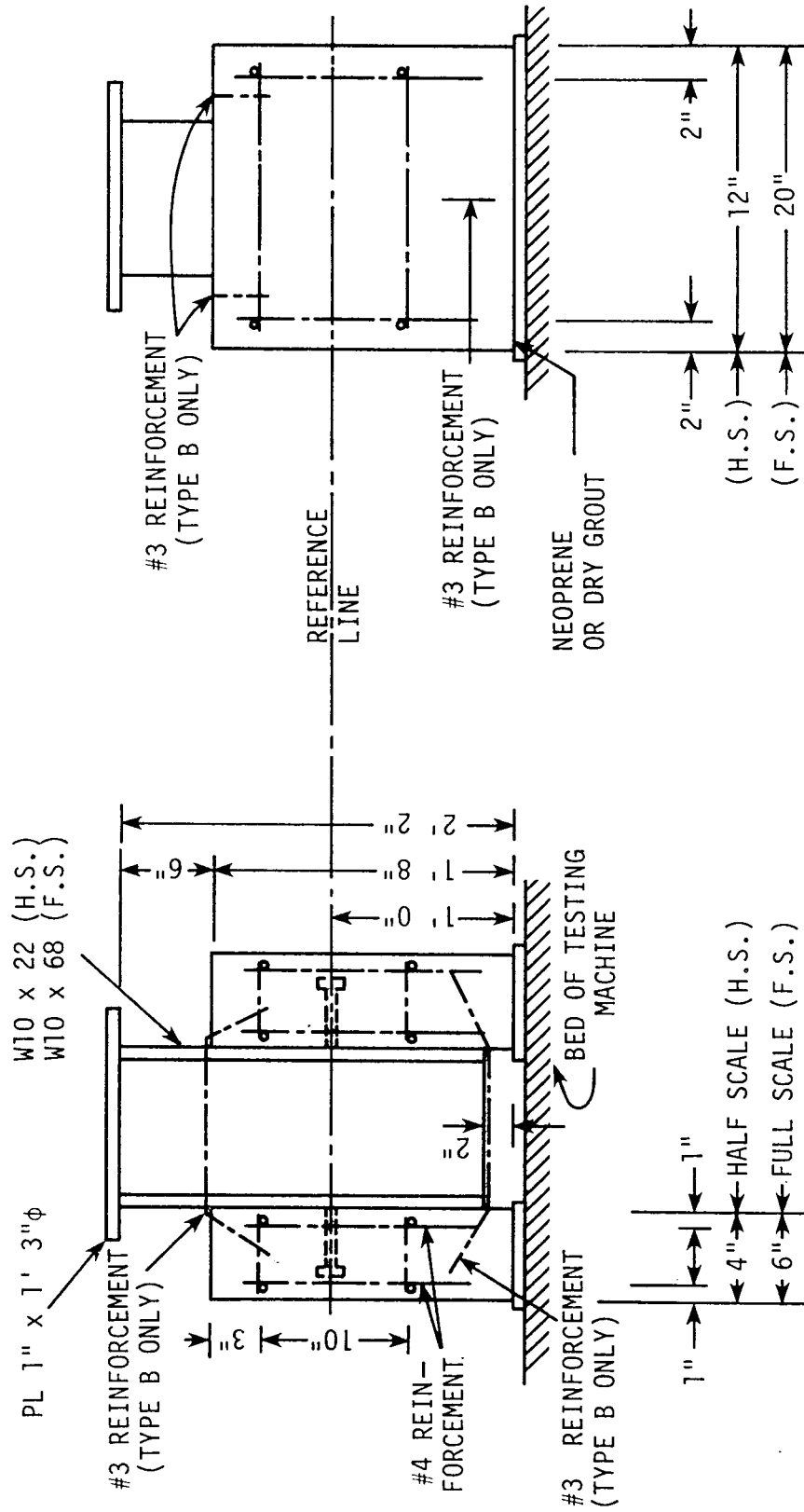
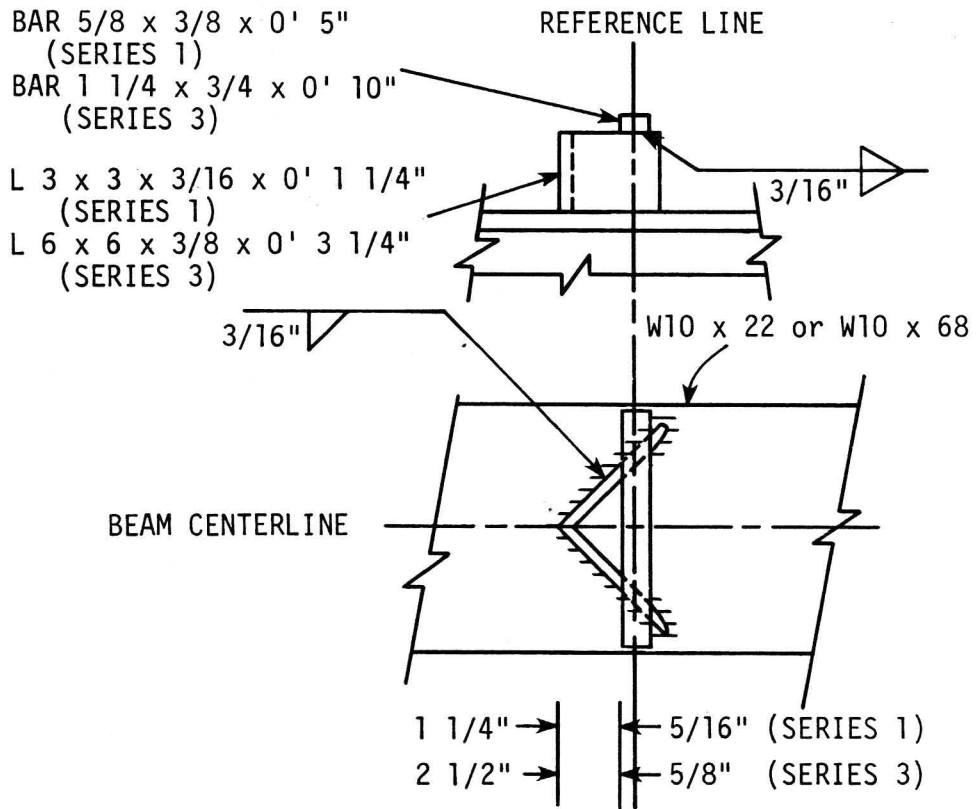
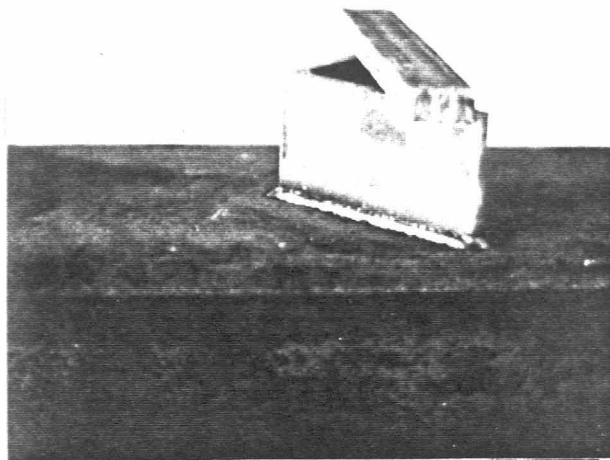


Fig. 1. Details and dimensions of the push-out specimen

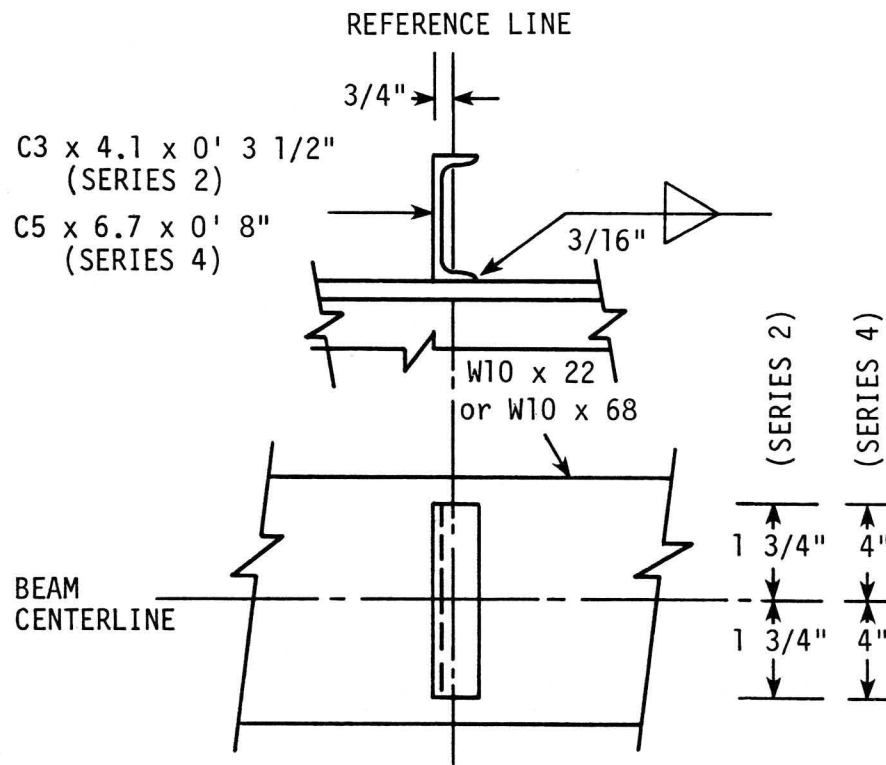


a. Details of half-scale (SERIES 1) and full-scale (SERIES 3) connector

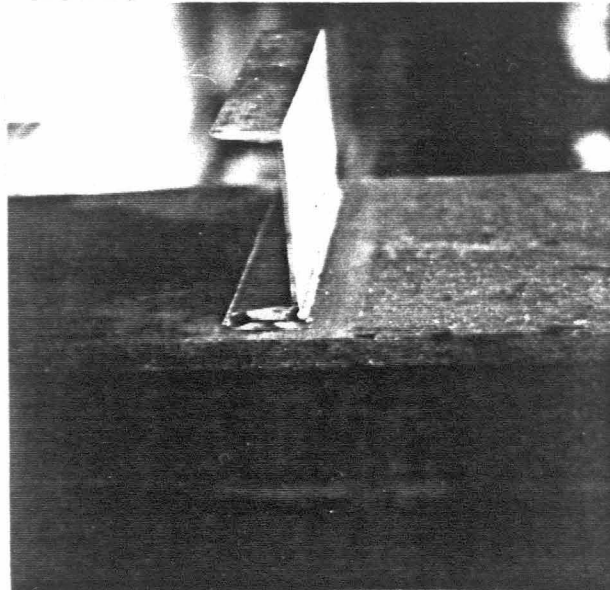


b. Photograph of full-scale connector

Fig. 2. Angle-plus-bar shear connector (Series 1 and 3)

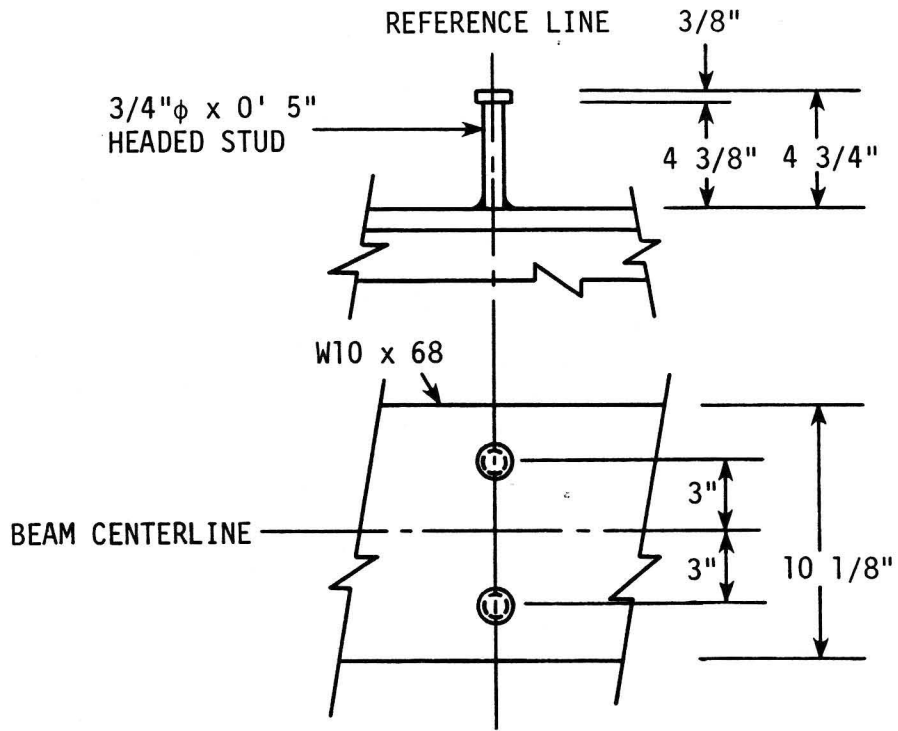


a. Details of half-scale (SERIES 2) and full-scale (SERIES 4) connector

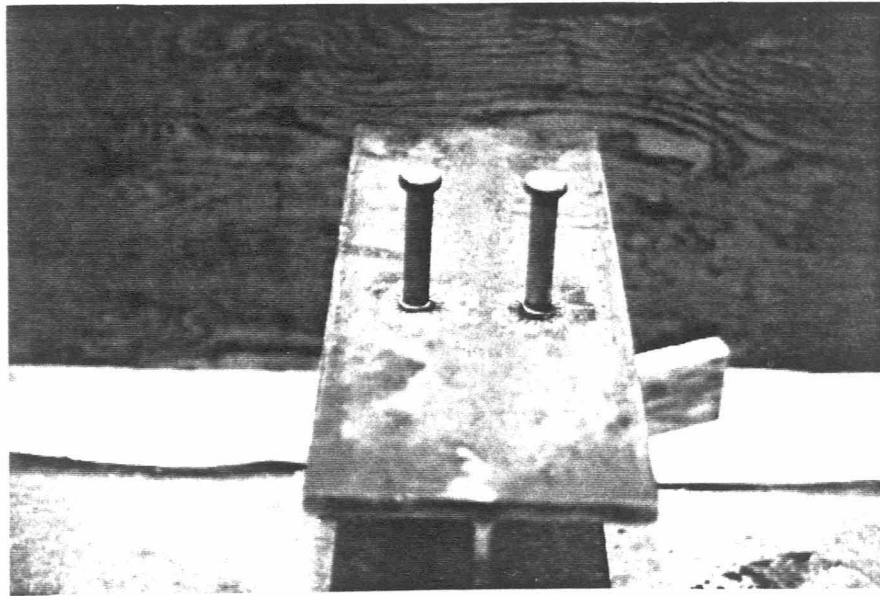


b. Photograph of full-scale connector

Fig. 3. Channel shear connector (Series 2 and 4)

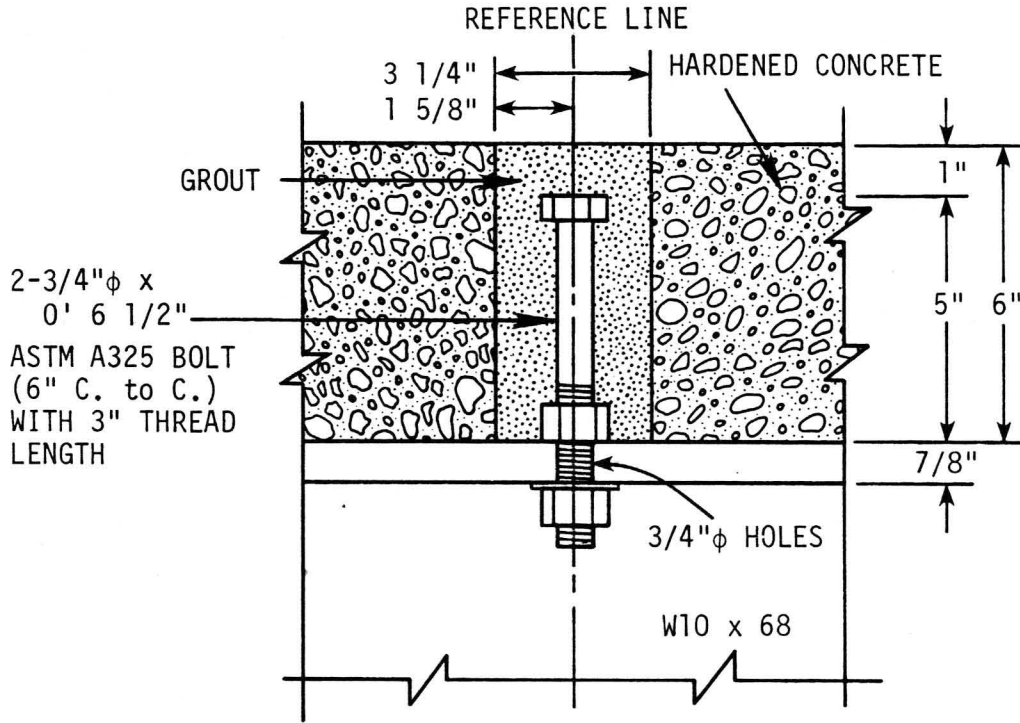


a. Details of full-scale stud connector

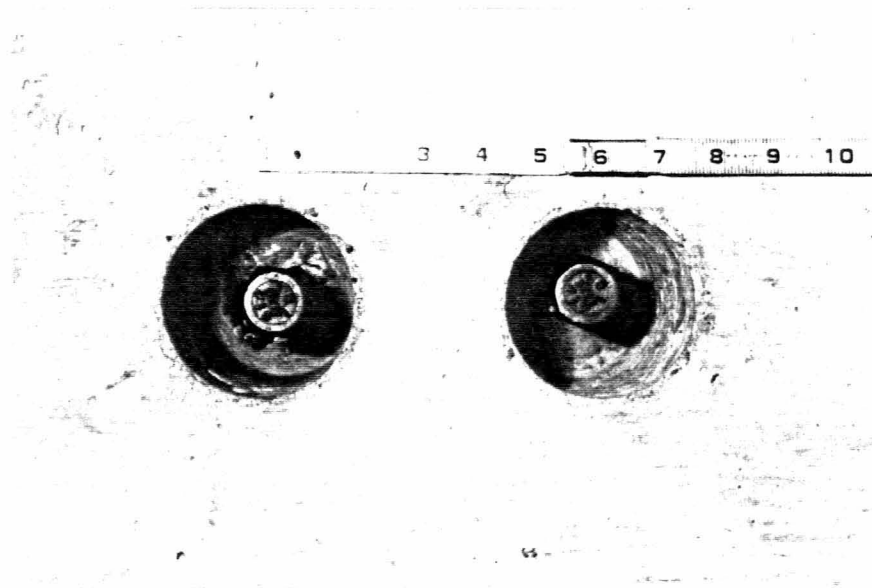


b. Photograph of stud connector

Fig. 4. Stud shear connector (Series 5)

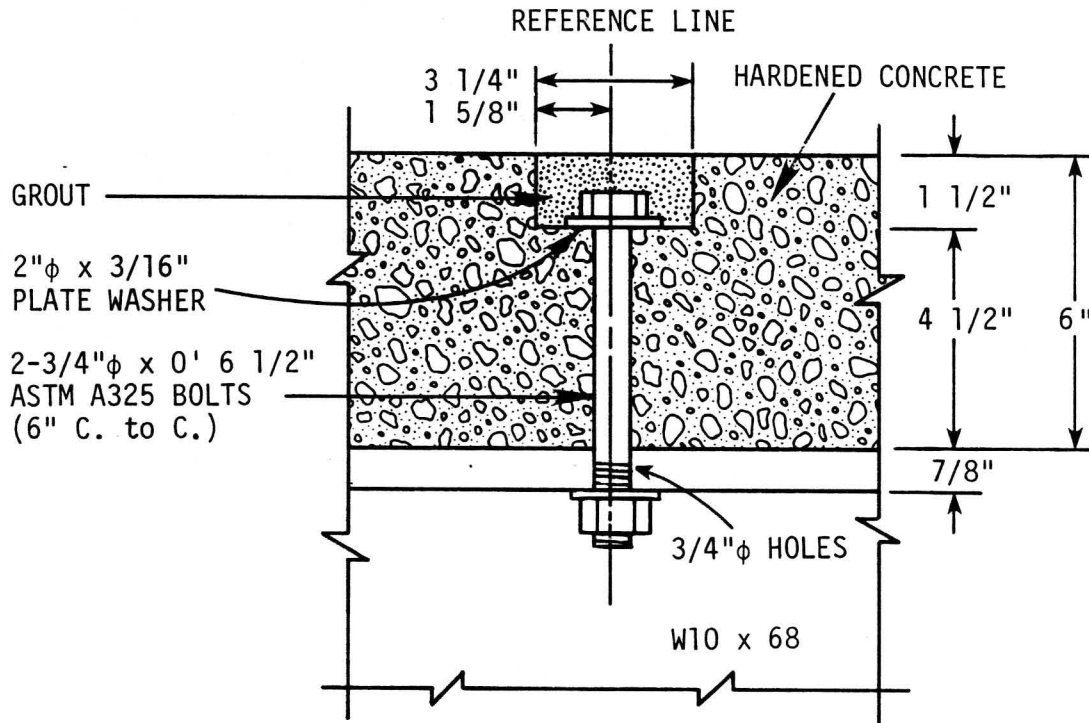


a. Details of double-nutted high strength bolt shear connector

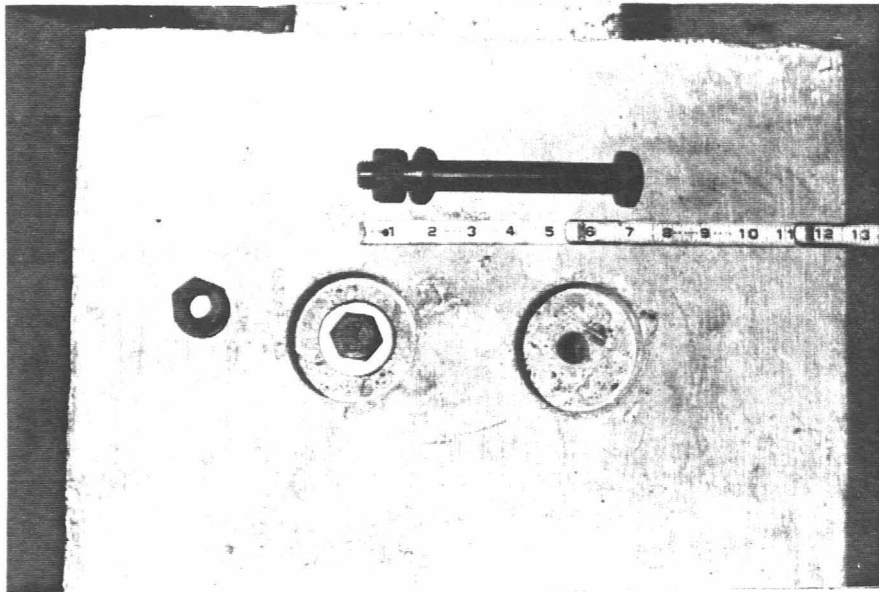


b. Photograph of double-nutted connector prior to placement of grout

Fig. 5. Double-nutted high strength bolt shear connector (Series 6)



a. Details of epoxied high strength bolt connector



b. Photograph of connector prior to installation of the bolts
Fig. 6. Epoxied high strength bolt shear connector (Series 7)

Table 1. Summary of push-out specimens tested

SERIES	TYPE	CONNECTOR DESCRIPTION	SPECIMENS
1	A	half-scale angle-plus-bar	HA1 HA2 HA3
2	A	half-scale channel	HC1 HC2 HC3
3	A	full-scale angle-plus-bar	FA1 FA2 FA3
4	A	full-scale channel	FC1 FC2
5	A	full-scale stud	FS1 FS2 FS3
6	B	double-nutted high- strength bolt	N1 N2 N3 N4
7	B	epoxied high-strength bolt	E1 E2 E3 E4

currently in use on various composite bridges and on the half-scale bridge of Phase I, while Type B specimens modeled techniques of adding shear connectors to existing bridges. Because the type of steel on several of the bridges requiring strengthening is unknown, only shear connectors that can be added by bolting rather than welding were tested.

Table 1 presents a breakdown of the push-out specimens grouped according to specimen series and type. As shown, Type A specimens were designated by two letters and one number. The first letter designates the specimen size; H for half-scale and F for full-scale. The second letter indicates the type of connector welded to the flange: S represents stud, A for angle-plus-bar, and C for channel. The number distinguishes between the various specimens in a given series.

Type B specimens were all full-scale specimens and, therefore, designated by just a letter and a number. The letter represents the process used for attaching the slab to the beam flange by bolting: E for epoxied and N for double-nutted. The number distinguishes between specimens within a series. As may be seen, Series 1 through 5 were Type A specimens and Series 6 and 7 were Type B specimens.

Earlier research had shown that the bond doesn't change the specimen's ultimate strength (17). Thus, although the beam flanges and shear connectors were thoroughly cleaned with a wire brush and then with acetone, no attempt was made to destroy the natural bond between the concrete and steel.

2.1.2 Fabrication of Specimens

A general description of the push-out specimens was given in the previous section. The following two sections, Section 2.1.2.1 and Section 2.1.2.2, present the fabrication procedures used for the Type A and the Type B specimens, respectively.

2.1.2.1 Type A Specimens The first step in the fabrication of the specimens was welding the shear connectors to the beams. Channel and angle-plus-bar connectors were welded utilizing a standard weld while the studs were installed using a Nelson stud welder. The location of the shear connectors in the various specimens may be determined by correlating the reference line in Figures 2 through 6 with the reference line in Figure 1.

The push-out specimens were cast vertically; rather than horizontally, so that both slabs could be cast from the same batch of concrete in order to omit any variation in concrete strength from one slab to another. Concrete was mixed in a 9 cu. ft. mixer in the structures laboratory and cast into the forms in three individual lifts. Each lift was thoroughly vibrated; care was taken to minimize the formation of voids adjacent to the shear connectors. Forms were fabricated so that three specimens could be cast simultaneously, as shown in Figure 7. Each slab was provided with a small amount of reinforcement, two layers of #4 reinforcement, arranged as shown in Figure 1.

A minimum of three 6 in. diameter x 12 in. long standard ASTM quality test cylinders were made during each pour. The specimens, as

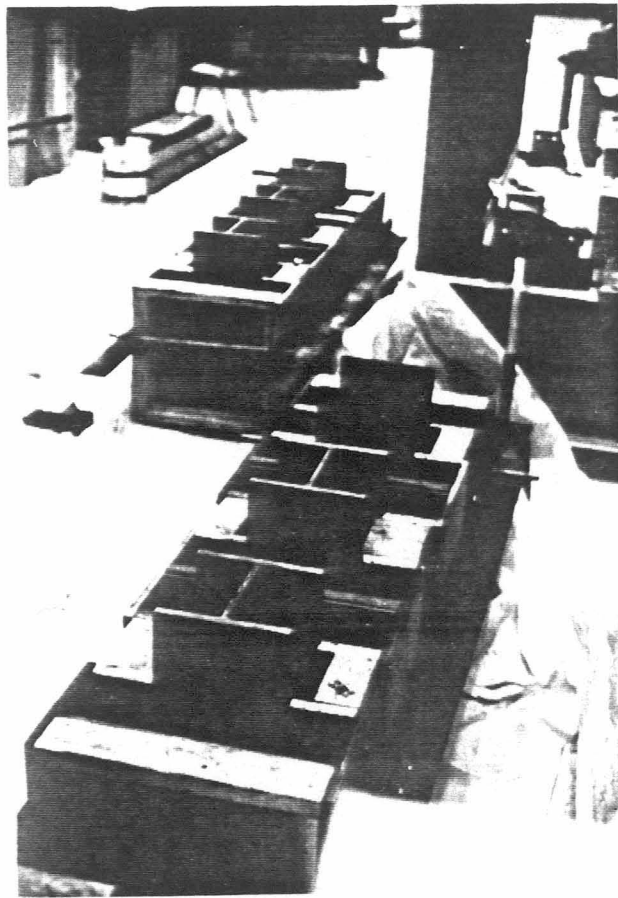


Fig. 7. Formwork used for constructing the push-out specimens

well as the control cylinders, were covered with burlap and plastic then wet cured for 5 to 7 days. Due to time constraints, the specimens needed to be tested before 28 days had elapsed. Therefore, a high-strength concrete was employed. From the nine day compressive strength determined, the specimens were found to be sufficiently strong for testing at an age of 14 days. Compressive strength values for all Type A specimens are presented in a later section.

2.1.2.2 Type B Specimens Fabrication of Type B specimens began with the vertical casting of slabs in the same formwork used for Type A specimens (Figure 7). A nominal amount of reinforcement was provided, as well as three #3 reinforcing bars as labeled and shown in Figure 1. The #3 reinforcing bars provided temporary connection of the slab to the beam flanges until the high-strength bolt shear connectors were in place. Prior to testing, the #3 reinforcing bars were removed, so that the only connection between the slabs and wide flange beam sections was provided by the high-strength bolts. Because all the specimens were full-size, concrete was purchased from a local ready-mix plant rather than mixing it in the laboratory as was done for the half-scale, Type A specimens which required smaller aggregate. The concrete was placed in two lifts, each of which was properly vibrated to prevent honeycombing.

Four 6 in. diameter x 12 in. long standard ASTM quality test cylinders were made for each set of three specimens. The specimens and cylinders were then covered with burlap and plastic and wet-cured

for 7 days. Due to the time required for the more involved fabrication of Type B specimens, Series 6 specimens were tested 41 days after the concrete was cast and Series 7 specimens were tested 52 days after casting. Appropriate compressive strength values are presented later.

After the formwork was removed, each specimen was rotated so that one slab was resting on the floor and the other resting on the beam section so the desired shear connectors could be added. Two different methods of adding high-strength bolt shear connectors to existing beams were investigated for ease of installation, ultimate strength and characteristics of load-slip and load-separation.

The first fabrication technique examined was the double-nut configuration depicted in Figure 5. Two 3 1/4 in. diameter x 6 in. deep cores, at 6 in. center to center, were drilled into each slab of the Series 6 specimens. Location of the cores along the length of the beam is given by the reference lines in Figure 1 and Figure 5. The concrete cores were removed and a 3/4 in. diameter hole was drilled through the beam flange at the center of each core. The side walls of the core holes were then roughened and cleaned to improve the bonding between the nonshrink Five Star grout and the hardened concrete. Acetone was used to remove the oil residue left from drilling the steel beams; water was used to remove the cementitious materials resulting from the coring.

High-strength bolts (ASTM A325 3/4 in. diameter x 6 1/2 in. long) were then placed in the holes through the beam flange and adjusted for

an overall length of 5 in. above the flange. Bolts were then tightened to the beam flange in a double-nut configuration. To retard the hydration process in the grout, the core walls were rinsed with water immediately prior to placement of the grout.

When the grouting was placed, three 3 in. diameter x 6 in. long standard ASTM quality test cylinders were made for determining the compressive strength. The grouting and cylinders were wet-cured for 4 to 5 days.

The addition of shear connectors to Series 7 specimens followed a different procedure, as portrayed in Figure 6. Two 3 1/4 in. diameter x 1 1/2 in. deep cores, at 6 in. center to center, were drilled into each slab. The reference lines of Figure 1 and Figure 6 locate the core holes along the length of the beam. At the center of each core, a 3/4 in. diameter core was drilled to the beam flange. After removal of all core material, a 3/4 in. diameter hole was drilled through the beam flange at each core location. The buildup of steel shavings in the 3/4 in. core caused the drilling to be halted frequently in order to remove the shavings. To provide an even bearing surface for the 1/8 in. plate washer and bolt combination, Five Star grout was placed in the 3 1/4 in. diameter core and leveled off 1 1/2 in. below the top surface of the slab. The grout used for leveling was allowed to wet cure for a minimum of 4 days.

In order to fill voids and provide bonding between the bolt and the slab, a concrete-steel epoxy was employed. The epoxy was spread

thoroughly over the shaft of a 3/4 in. diameter x 6 1/2 in. long ASTM A325 high-strength bolt. The epoxy-covered bolt was then placed in the 3/4 in. diameter core and moved vertically up and down to provide an even coating of epoxy between the core walls and bolt shaft. The bolts were immediately tightened, thus forcing out any voids in the viscous epoxy and providing uniform bonding between the steel and concrete.

The epoxy was allowed to cure for a minimum of 24 hours before Five Star grout was placed in the 3 1/4 in. diameter cores (Figure 6).

Two 3 in. diameter x 6 in. long standard ASTM quality test cylinders were made of the grout used in the previously described patching process. The patching on all specimens and the control cylinders were wet-cured for a minimum of 4 days.

2.1.3 Loading Apparatus and Instrumentation

Slip and separation between the slabs and the beams were measured on all push-out specimens. The instrumentation for all specimens consisted of eight deflection dials, located as shown in Figure 8. Four deflection dials recorded slip and the remaining four deflection dials measured separation at two elevations along the slab.

The four deflection dials (used to measure slip) were rigidly attached to the web of the beam as shown in Figure 8. The stem of each deflection dial was allowed to bear against blocks attached to the slab as shown. Slip was measured relative to the centerline of the various shear connectors.

The remaining four deflection dials, used to measure separation

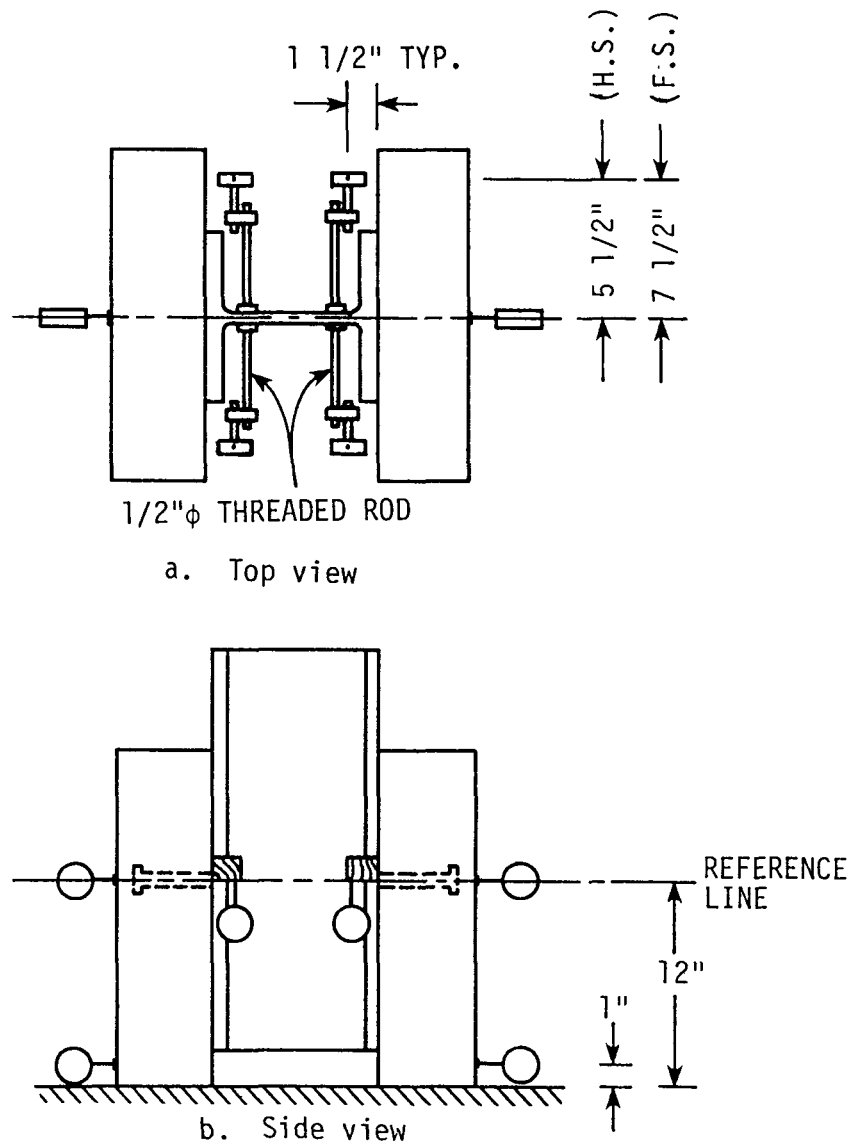


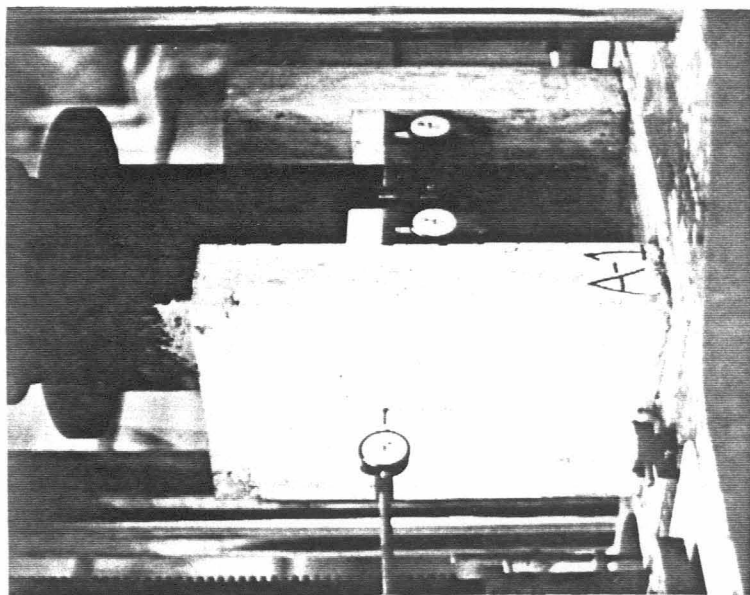
Fig. 8. Location of instrumentation used in the push-out tests

or "uplift," were rigidly attached to the platen of the universal testing machine. As shown in Figure 8, separation was measured at the connector centerline and 1 in. from the end of the slab bearing on the testing machine platen.

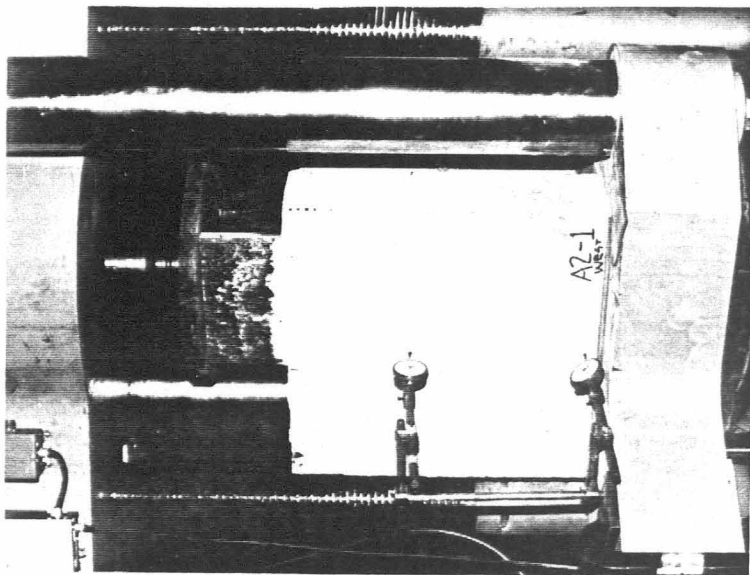
The arrangement for testing in the universal testing machine is shown in the photographs of Figure 9. Placement of the half-scale test specimen in the testing machine is shown in Figure 9a and for the full-scale test specimen in Figure 9b. For uniform load distribution, the lower ends of the slabs were bearing either on a 1/4 in. thick pad of neoprene or a thin layer of dry Portland cement. Load was applied to the upper end of the steel beam by the head of the testing machine through a steel distribution plate. A 3/4 in. diameter steel ball was placed between the head of the testing machine and steel plate on the half-scale specimens to provide concentric loading. When the full-scale specimens were tested, the steel ball was removed due to the higher loads involved. To restrain the slabs in the event that sudden failure occurs, rope was wrapped around the various specimens during testing.

2.2 Composite Beam Tests

As has previously been mentioned, the half-scale model bridge, constructed during Phase I of this study, was cut into four individual beams. The physical description, as well as the loading and instrumentation of the four composite beams, is presented in the following sections.



a. Half-scale specimen



b. Full-scale specimen

Fig. 9. Photographs of push-out specimens in place for testing

2.2.1 Description of Specimens

The four composite steel beam/concrete slab specimens were fabricated from the half-scale model bridge from Phase I. The model bridge framing plan and midspan cross-section may be found in Reference 11. The composite beam specimens were obtained by making five longitudinal cuts in the model bridge as depicted in Figure 10. The cuts were made with a gasoline-engine powered concrete saw which was provided and operated by personnel from the Iowa Department of Transportation.

Two of the beams, Beams #1 and #4 (Figure 10), had a nominal slab width of 1 ft 5in. and were exterior-type composite beams with a flange on one side only. The remaining beams, Beams #2 and #3, had a nominal flange width of 4 ft 10 in. and were interior-type composite beams with equal widths of slab on each side of the beam centerline. Flange widths on Beams #2 and #3 were made equal to the stringer spacing, thus minimizing the number of saw cuts required. Flange widths on Beams #1 and #4 were determined by calculating the width of slab needed to locate the centroid of the slab about a vertical axis through the centerline of the steel beam. This was done to decrease the possibility of unsymmetrical bending. The actual composite beam slab widths, given in Figure 11 and Table 2 along with the average slab thicknesses, were the result of inaccuracies in the cutting process.

All four beams were equipped with the post-tensioning system used in the testing of the model bridge of Phase I. Post-tensioning forces of various magnitude were applied during testing of the beams by stressing the Dywidag Threadbars on each beam. Details of the post-

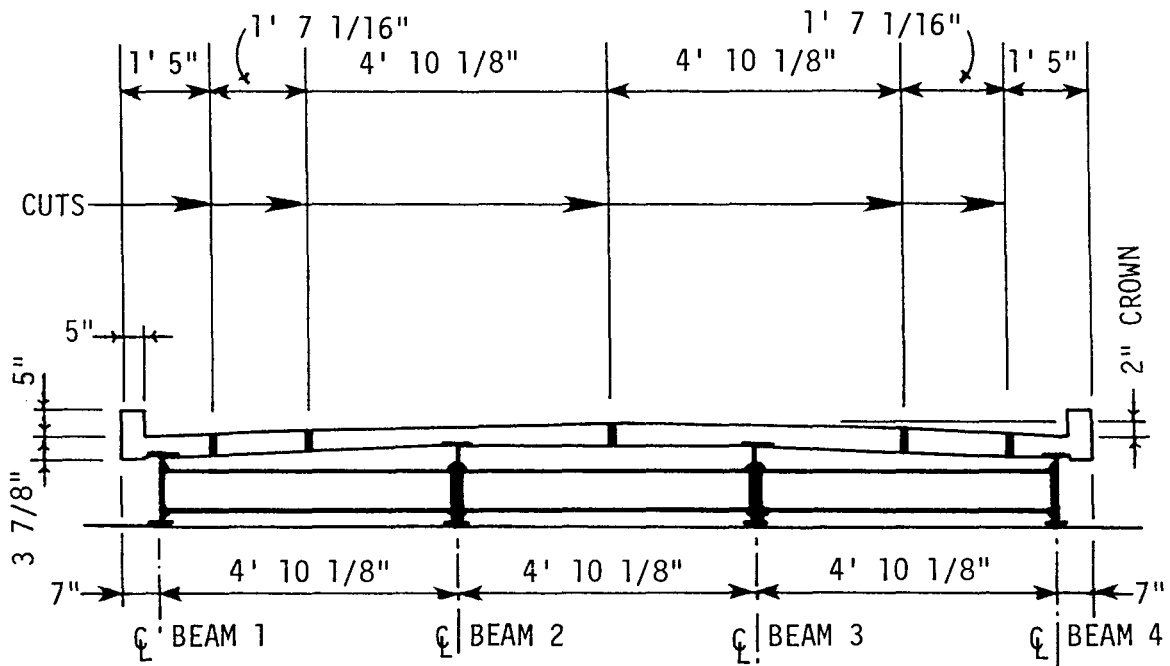
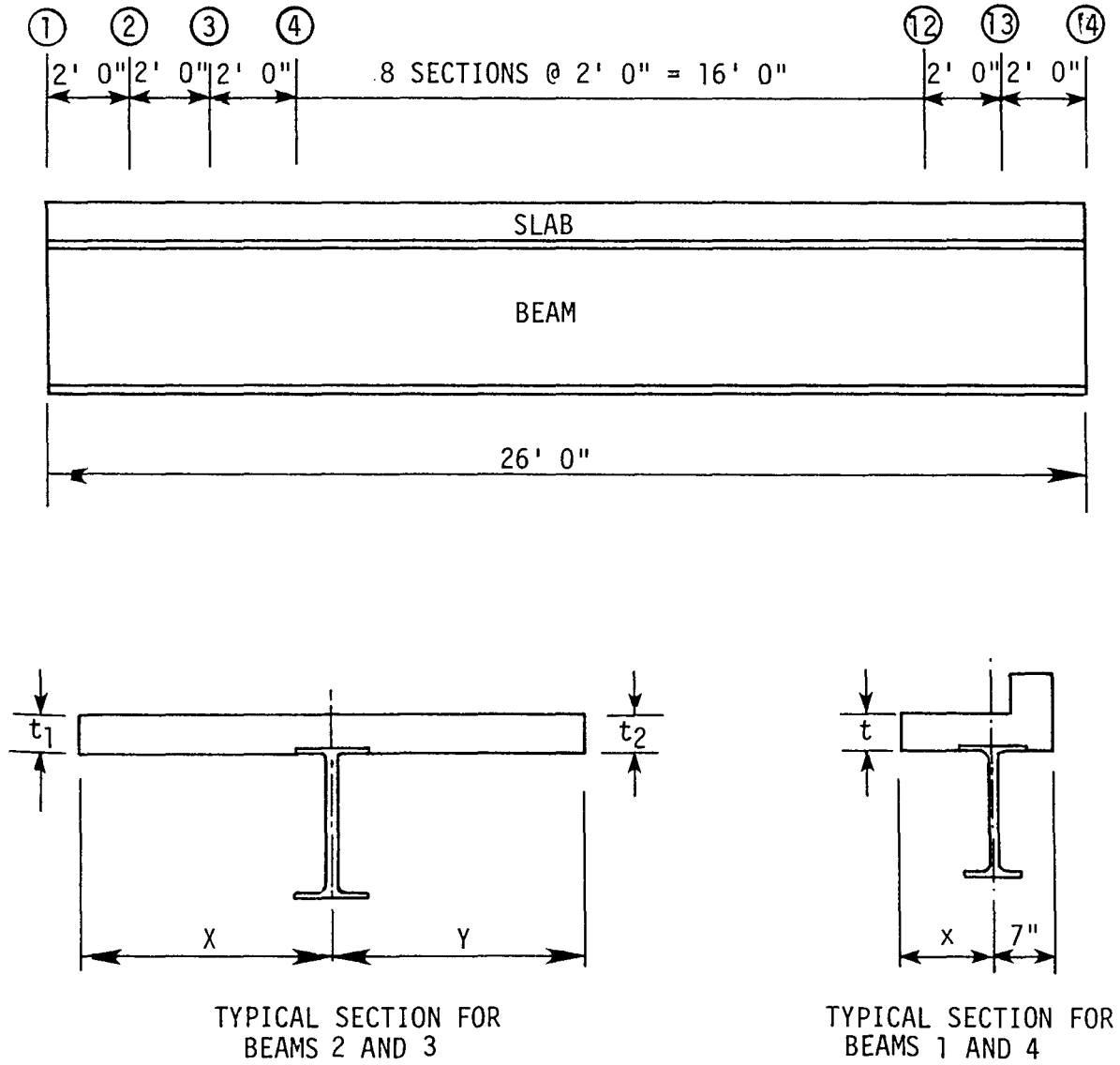


Fig.10. Cross-section of model bridge showing the location of longitudinal cuts



where, $T = \frac{t_1 + t_2}{2}$

Fig.11. Location of composite beam sections where measurements of slab width and thickness were determined (See Table 2 for values of each variable)

Table 2. Actual widths for each composite beam tested

BEAM #1			BEAM #4		
POINT	x ^a (IN.)	t ^a (IN.)	POINT	x ^a (IN.)	t ^a (IN.)
1	10.50	4.25	1	10.00	4.00
2	10.25	4.25	2	10.00	4.00
3	10.25	4.38	3	10.00	4.12
4	9.62	4.25	4	10.00	4.00
5	9.25	4.12	5	10.00	4.12
6	9.62	4.12	6	10.00	4.25
7	10.25	4.12	7	10.25	4.12
8	10.38	4.25	8	10.12	4.12
9	10.50	4.12	9	10.00	4.12
10	10.62	4.12	10	9.75	4.00
11	10.38	4.12	11	9.50	4.12
12	10.62	4.12	12	9.75	4.00
13	11.00	4.12	13	10.12	4.00
14	11.25	3.88	14	10.62	3.88
AVE.	10.32	4.16	AVE.	10.01	4.07

^aRefer to Fig. 11 for definition of x, t, X, Y, and T.

Table 2 (continued)

BEAM #2				BEAM #3			
POINT	X ^a (IN.)	Y ^a (IN.)	T ^a (IN.)	POINT	X ^a (IN.)	Y ^a (IN.)	T ^a (IN.)
1	31.12	28.50	4.22	1	28.00	28.62	4.06
2	31.12	28.62	4.25	2	28.62	28.62	4.06
3	31.12	28.62	4.19	3	28.75	28.25	4.00
4	31.00	28.50	4.16	4	28.62	27.88	4.06
5	31.00	28.50	4.09	5	28.50	27.62	4.06
6	31.12	28.38	4.09	6	28.50	27.38	4.19
7	31.00	28.25	4.06	7	28.50	27.25	4.19
8	31.00	28.12	4.16	8	28.38	27.00	4.12
9	30.75	28.12	4.16	9	28.62	27.00	4.06
10	30.62	28.25	4.06	10	29.00	27.12	4.06
11	30.38	28.25	4.03	11	28.88	27.12	4.19
12	29.88	28.38	4.00	12	28.88	27.12	4.12
13	29.62	28.75	4.06	13	28.62	27.00	4.19
14	29.50	29.00	4.12	14	28.62	27.25	4.12
AVE.	30.66	28.45	4.12	AVE.	28.61	27.52	4.11

tensioning system employed may be found in Reference 11.

The properties of the concrete and steel in the four beams, although also available in Reference 11, are presented in Tables 3 and 4 for convenient reference.

The shear capacity of the beams was less than that required by AASHTO bridge standards (1). Therefore, additional shear connectors (high-strength bolts double-nutted to the top flange) were added to one interior beam, Beam #3, and one exterior beam, Beam #4. The locations of the existing angle-plus-bar shear connectors for all four composite beams are given in Reference 11; the locations of the shear connectors added to Beam #3 and Beam #4 are shown in Figure 12.

These locations were dictated by the location of the existing angle-plus-bar connectors. Core holes were located on either side of the beam centerline; however, this placement was varied slightly on the exterior beams so that the cores did not have to pass through the curbs. For ease of construction, the core holes (3 1/4 in. diameter) were drilled before the bridge was cut into individual beams.

The additional shear connectors were 1/2 in. diameter x 4 in. long ASTM A325 high-strength bolts. The bolts were double-nutted to the beam flange similar to the configuration (shown in Figure 5) used in the Series 6 push-out specimens. An ultimate strength value for the existing angle-plus-bar shear connector was computed using data obtained from the push-out tests. The total resisting force of the angle-plus-bar connectors was then determined for each beam and

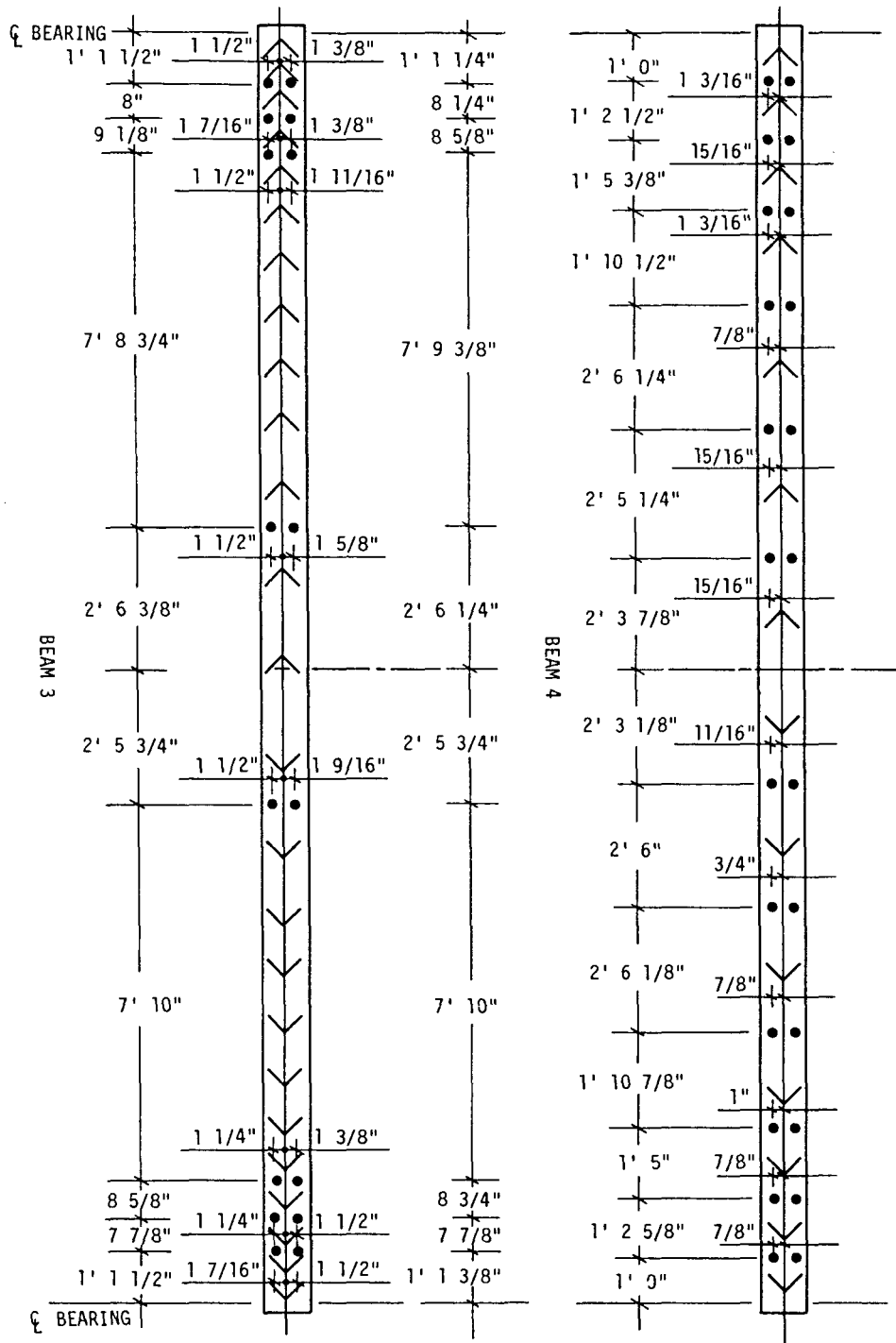
Table 3. Physical properties of concrete

	f'_c (psi)	E (ksi)
Deck	3300	2830
Curb	7450	5080

Table 4. Physical properties of steel

	σ_y (ksi)	σ_{ult} (ksi)	E (ksi)
Reinforcement			
#3	69.8	110.8	29,100
#4	70.8	109.7	-
Prestressing	-	156.1	24,100
W16 x 26	44.1	66.9	29,990
W14 x 22	44.7	69.4	28,990

Fig. 12. Location of high-strength bolt shear connectors added to Beams #3 and #4

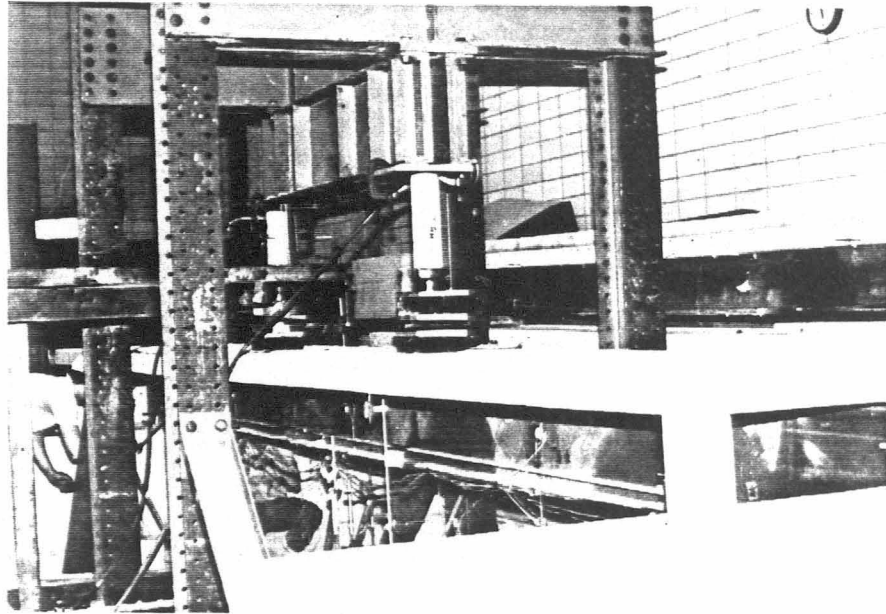


was found to be less than that required. Therefore, sufficient bolt connectors were added to one interior and one exterior composite beam to increase the shear capacity to the required level. The ultimate strength of the bolts was calculated using the welded stud formula for shear connectors in the AASHTO standards (1). From the laboratory work performed on the push-out specimens, this was found to be slightly conservative.

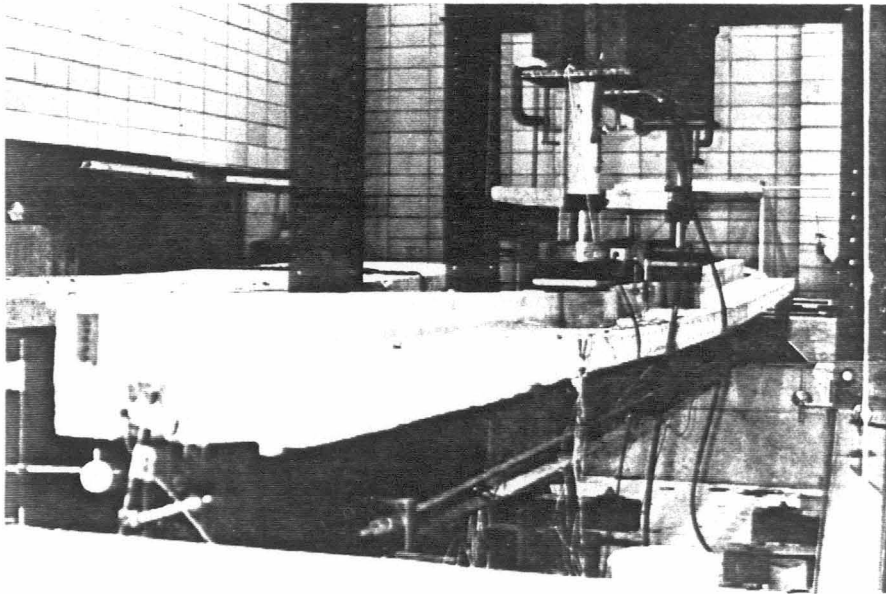
2.2.2 Loading Apparatus and Instrumentation

This section outlines the loading apparatus and instrumentation employed on the four test specimens. The same loading apparatus, except for slight variations in the load point location, was used in all tests. The instrumentation was nearly identical on each of the composite beams.

Load was applied to the beams through two 100 kip hydraulic jacks bearing against a steel frame anchored to the structural testing floor. Photographs of the test set-up used on the interior and exterior beams are shown in Figure 13a and 13b, respectively. The load points were nominally 80 in. apart; however, the exact locations may be found in Figure 14 along with other details of the test set-up. In order to transmit force uniformly to the slab, a combination of steel plates and neoprene pads was placed between the jacks and the slab. To transmit force through the curb and slab on the exterior-type composite beams, a concrete block was placed under the neoprene pads. Force was then transmitted through the concrete block and curb, which were at the same

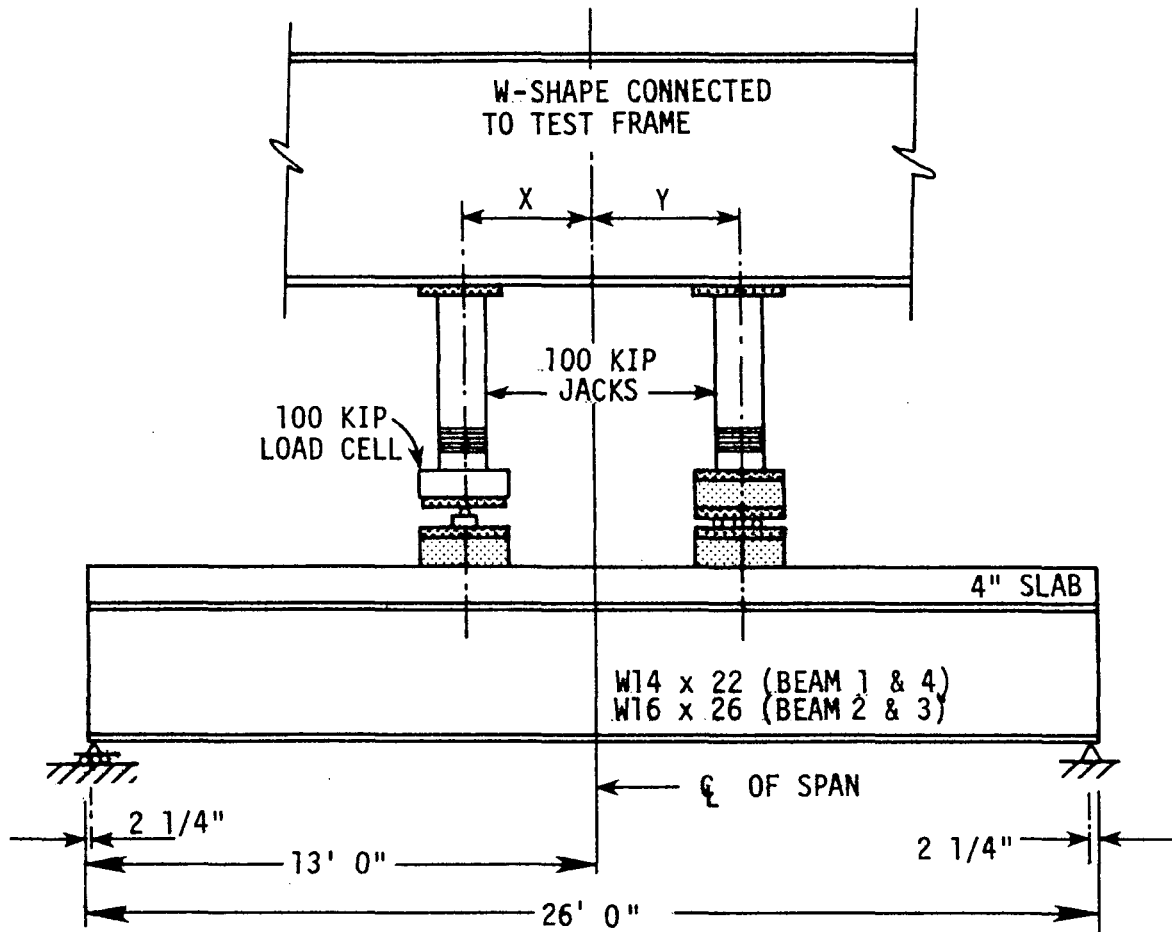




a. Interior beam specimen



b. Exterior beam specimen

Fig. 13. Photographs of composite beam test set-up showing test frame and specimen in place



-  PL - 1" x 9" x 9"
 3" x 9" x 9" NEOPRENE PAD

BEAM	X	Y
1	39 3/4"	40"
2	40"	40"
3	38 7/8"	40 1/2"
4	39 1/2"	39 3/4"

Fig. 14. Loading apparatus employed for testing the composite beams

elevation. To prevent horizontal restraint at the load points, pin and roller supports were provided under the jacks. The jack pin support coincided with the beam's roller support and the jack roller support with the beam's pin support; details of the load points are provided in Figure 14.

The load on the specimen was measured by a 100 kip load cell and checked by hydraulic jack pressure. The load cell was placed under the jack pin support (Figure 14) and values of load were recorded by the data acquisition system. Loads determined by jack pressure were in good agreement with those determined using the load cell.

Post-tensioning load was applied by two 60 kip hydraulic jacks. As was done in Phase I, the post-tensioning force was accurately determined through the use of strain gages mounted on the tendons.

Instrumentation for all tests consisted of mechanical displacement dial gages, electrical-resistance strain gages, and direct current displacement transducers (DCDTs). DCDTs were used to measure relative movement between the steel beam and concrete slab, or relative slip, as well as the deflection at three locations. At all other locations, displacements were measured with mechanical displacement dial gages, henceforth referred to as deflection dials.

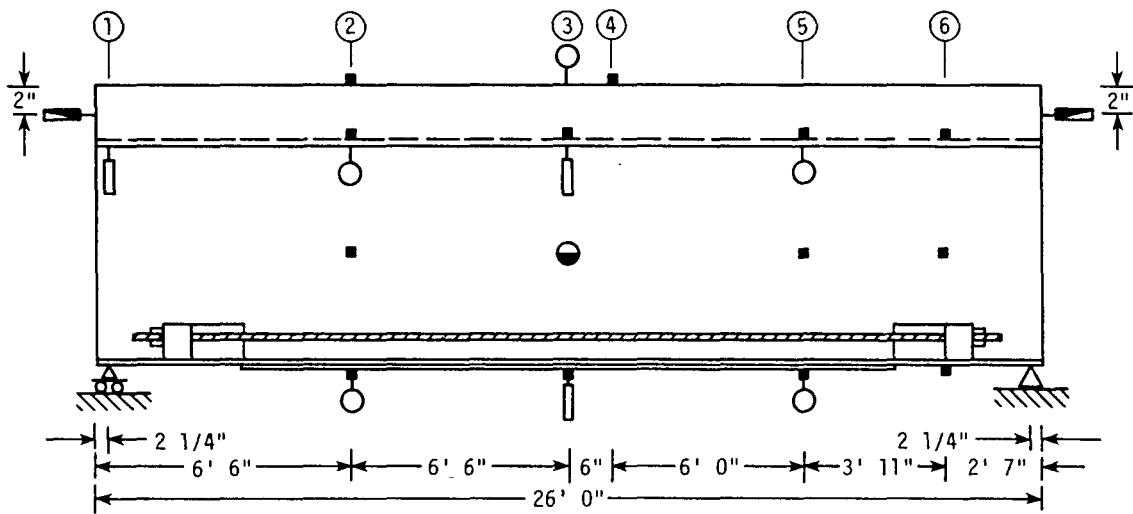
Electrical-resistance strain gages, henceforth referred to as strain gages, were attached to the steel and concrete wherever measurement of strains was desired. The strain gages were installed in the normal manner with recommended surface preparation and adhesive. The majority of the strain gages were installed during Phase I (i.e., on the model

bridge) while the remaining strain gages were mounted after the composite beam specimens had been fabricated. All the strain gages were self-temperature compensated and provided with three-wire leads to minimize the effect of the long lead wires and any temperature changes. DCDT and strain gage measurements were read and recorded by the data acquisition system, while deflection dial measurements were recorded manually.

All four composite beams, as may be seen in Figures 15 and 16, were tested as simply supported beams. Also shown in these figures are the locations of the strain gages, deflection dials, and DCDTs used in each of the composite beam tests; note the DCDTs located at the ends of each beam to measure relative slip. The total number of DCDTs, strain gages, and deflection dials employed on each composite beam is given in Table 5.

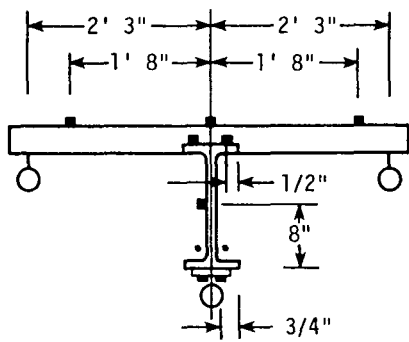
Table 5. Total number of DCDTs, deflection dials, and strain gages on each composite beam

BEAM NO.	DCDTs	DEFLECTION DIALS	STRAIN GAGES
1	5	8	16
2	5	7	18
3	5	7	26
4	5	8	29

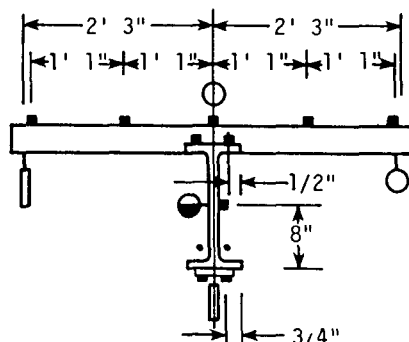


SIDE VIEW

SYMBOL	TYPE OF MEASUREMENT	GAGE
	VERTICAL DISPLACEMENT	DCDT
	RELATIVE SLIP	DCDT
	VERTICAL DISPLACEMENT	DEFLECTION
	HORIZONTAL DISPLACEMENT	DEFLECTION
	STRAIN	STRAIN

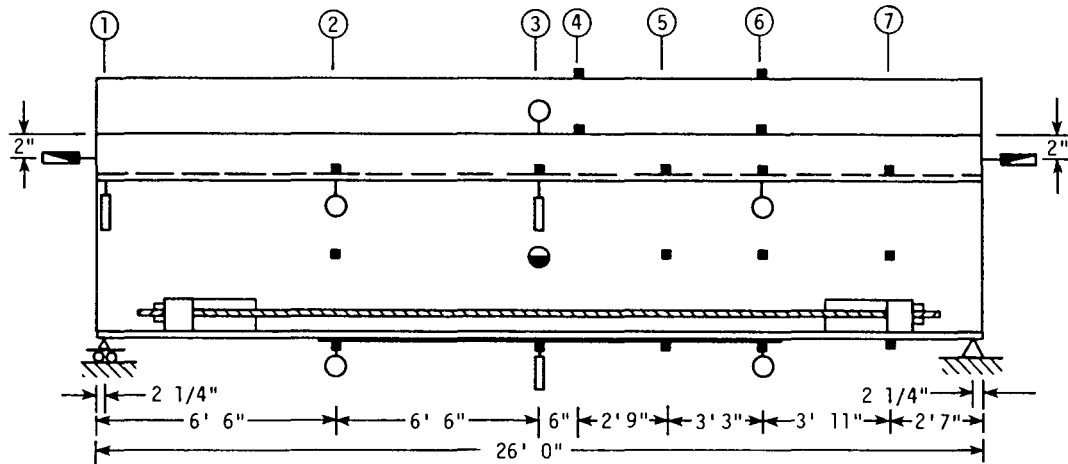


TYPICAL SECTION



SECTION 3 - 3

Fig. 15. Location of instrumentation on Beams #2 and #3



SIDE VIEW

SYMBOL	TYPE OF MEASUREMENT	GAGE
	VERTICAL DISPLACEMENT	DCDT
	RELATIVE SLIP	DCDT
	VERTICAL DISPLACEMENT	DEFLECTION
	HORIZONTAL DISPLACEMENT	DEFLECTION
	STRAIN	STRAIN

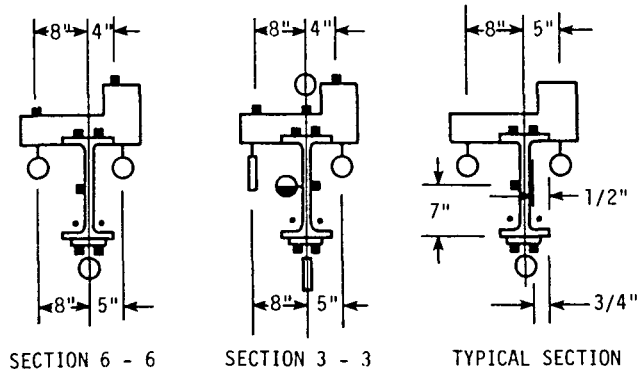


Fig. 16. Location of instrumentation on Beams #1 and #4

3. TESTS AND TEST PROCEDURES

This section outlines the details of the specific tests. Each test program (i.e., push-out tests and composite beam tests) consisted of several individual tests. In this section, only test set-ups will be discussed; interpretation and discussion of results will be presented in Section 4.

3.1 Push-Out Tests

The tests involving both Type A and Type B push-out specimens proceeded in the same general manner. Testing began with a pre-load of approximately 10% of the predicted ultimate load for each specimen. The pre-load value of 10 to 25 kips was applied for a variety of reasons: to insure an even distribution of force through the proper seating of the steel distribution plate on the beam flanges, to check the operation of the deflection dials, and to break the bond between the concrete and the steel beam.

By destroying the bond, consistent ultimate load results will occur because the entire load is on the connectors (17). The bond was physically destroyed even though it has been reported that shrinkage of the concrete is sufficient to destroy bond (18). Previous research (14) has indicated that the load-slip relationship will not be affected by unloading and reloading the specimens.

After the pre-load had been released and equilibrium in the system established, the load was applied in increments of varying magnitude.

The magnitude of the increments for the tests varied from 10 kips to 50 kips at the beginning of the tests and 1 to 5 kips when failure was imminent. After each increment of load, slip and separation displacements were recorded. At higher values of load, the load was held constant so that behavior (e.g., crack patterns) could be recorded. When failure occurred, photographs were taken to show the final deformed shape and the ultimate load was recorded. The specimens were then removed from the testing machine and disassembled to determine the effects of the loading on the slabs and shear connection. The duration of each test was approximately 40 minutes; the set-up time for each test varied from 1 to 2 hours.

3.2 Composite Beam Tests

As has previously been mentioned, numerous tests were performed on each composite beam. Test variables included magnitude of the initial post-tensioning force and magnitude of vertical load. Four tests were performed on each beam; the magnitude of test variables, as well as the combination of variables in each test, is summarized in Table 6. A description of the four tests performed on each beam, as well as occurrences and test set-ups unique to the individual composite beams during execution, is provided in the next two sections (Section 3.2.1 discusses elastic range tests, Tests A, B, and C, while Section 3.2.2 covers the ultimate strength tests, Test D).

To distinguish between tests, a number and a letter are used to designate each test. Thus, Test 3A indicates the Test A of Beam #3.

Table 6. Summary of tests performed on the composite beam specimens

BEAM NO.	TEST	POST-TENSIONING FORCE (KIPS)	VERTICAL LOAD PER LOAD POINT (KIPS)	
			MAXIMUM	INCREMENT
1	A	0	9	1
	B	12	9	1
	C	24	9	1
	D	34	35.0	1 ^a
2	A	0	18	1
	B	16	15	1
	C	32	15	1
	D	48	48.3	1 ^b
3	A	0	15	1
	B	16	15	1
	C	32	15	1
	D	48	50.4	1 ^b
4	A	0	9	1
	B	12	9	1
	C	24	9	1
	D	34	38.1	1 ^a

^aIncrement was increased to 2^k after the vertical load reached 9^k.

^bIncrement was increased to 2^k after the vertical load reached 15^k.

3.2.1 Elastic Range

The following sentences describe the testing procedures utilized in Tests A, B, and C on the four composite beams.

Initially in Test A, each composite beam was loaded with a pre-load of 1 to 2 kips to insure proper seating at the load points and to check the performance of all gages and DCDTs. After the preloading, initial "zero" readings for all strain gages, deflection dials, and DCDTs were recorded. As loading progressed, strain and displacement readings were taken after each load increment. As shown in Table 6, each composite beam was loaded to slightly less than the calculated elastic limit of the steel beam. Behavior was noted and photographs were taken throughout the test. After the load was released, beams were allowed to sit unloaded for a few minutes before final "zero" readings were recorded.

Tests B and C were slightly different from Test A in that a predetermined force was applied to the post-tensioning tendons (Table 6 for magnitude of post-tensioning force). Composite beam specimens were then pre-loaded, vertical load applied, and readings taken as was done during Test A. The procedure used to "lock in" the post-tensioning force was similar to that used in Phase I. Test length (approximately one hour) was controlled in order to minimize any variations in temperature and drift that may occur in the strain gages.

3.2.2 Ultimate Strength

The final test performed on each beam, Test D, consisted of applying vertical load to the post-tensioned beam until the ultimate capacity of the beam was reached. The test procedure up to the calculated elastic limit of the steel beam was identical to Tests B and C except that a higher post-tensioning force (Table 6) was locked into each composite beam. At the calculated elastic limit of the steel beam, the loading increment was increased to 2 kips per load point. Behavior of the beam was noted and photographs taken when significant deformations occurred and when failure occurred.

4. TEST RESULTS AND ANALYSIS

In Chapter 3, the details of the test program were presented. In subsequent sections of this chapter, the results of each test and events which occurred during each test will be summarized and an analysis of their significance presented. For clarity, each test will be discussed separately.

4.1 Push-Out Test Results and Analysis

Earlier, the push-out specimen descriptions (Section 2.1) and push-out test procedures (Section 3.1) were presented. The following sections will present behavioral information and data obtained from the various push-out tests. Experimental results obtained are then compared to theoretical values and to each other when relevant.

The data from the push-out tests consisted of slip and separation measurements, as well as ultimate load values for each specimen. The four slip readings obtained were averaged together to produce the average slip per connector. In the case of a stud or high-strength bolt shear connector, a connector consists of two studs or bolts. The load per connector is one-half the total load applied to the steel beam.

The separation between the concrete and steel was measured at two locations along the face of the slab. Deflection dials located 1 in. above the bed of the testing machine were used to check for excessive sliding of the specimen on the testing machine platen, as well as separation between the slabs.

The results from these dials indicated movement along the platen was occurring, but was of a small enough magnitude to neglect. Relative separation of the slabs at the base was found by averaging the two deflection dials. The separation at the base does not provide a true value of the "uplift" on the connectors but was checked to insure that it was small; separation was found to be small, and, thus, was not given any further consideration.

The average of the two deflection dials at connector level is also referred to as the uplift of the slab from the beam. This "uplift" or separation was checked to insure that it was "less than half the interface slip at the corresponding load level" (22); thus, closely approximating the uplift forces present in an actual composite beam. All but one connector, the angle-plus-bar, met the 50% limit. The rigid nature of the angle-plus-bar connector probably caused the excessive separation and will be discussed in more detail later. Because the uplift values obtained in the Series 2, 4, 5, 6 and 7 connectors were within the 50% limit (see typical load-separation curves in the Appendix), the effect of uplift was considered to have minimal influence on the behavior of these connectors.

4.1.1 Type A Specimens

As explained in Section 1.2.1, the Type A specimens were tested in order to obtain experimental values for angle-plus-bar connectors (used on bridges built from the 1940s to 1960s), welded studs, and channel

connectors. By comparing experimental results to existing design equations (1), a design rationale could be developed for the angle-plus-bar connectors. The use of two slab push-out specimens is generally accepted for the determination of the strength of shear connectors (2,13,22). Results obtained from push-out tests provide an upper limit to values used for the design of composite beams after the push-out test results are checked for any inconsistencies (18,22).

To eliminate several of the variables, concrete compressive strengths were held nearly constant and the physical dimensions of the push-out specimens were held constant. Table 7 presents compressive concrete strengths, experimental and theoretical ultimate loads, and types of failure for Series 1 through 5. Predicted ultimate load values for Series 2, 4, and 5 were obtained by using relationships from AASHTO (1); those for Series 1 and 3 were obtained by using a modified form of the AASHTO channel formula (1). As may be seen, within the various specimen series the experimental ultimate load values are very consistent as are the failure mechanisms (except for one case). This same consistency can also be seen in the load-slip curves for the individual specimens of a given series (see the Appendix).

The connector ultimate load values obtained experimentally compared very well to the predicted values for the half-scale specimens (Series 1 and 2). Referring to Table 7, the ratio of predicted to experimental ultimate load for the channel and angle-plus-bar connectors yielded results between 1.00 and 1.13. The slightly low

Table 7. Push-out tests: Summary of test results and predicted ultimate loads for Type A specimens

SPECIMEN DESIGNATION	COMPRESSIVE STRENGTH, f'_c PSI	OBSERVED CONNECTOR ULTIMATE LOAD, KIPS	PREDICTED ULTIMATE LOAD, KIPS	RATIO OF PREDICTED TO EXPERIMENTAL ULT. LOAD	TYPE OF FAILURE ^a
SERIES 1					
HA1	4110	38.0	42.1	1.11	D
HA2	4110	41.6	42.1	1.01	D
HA3	4110	42.0	42.1	1.00	D
SERIES 2					
HC1	4110	40.5	44.2	1.09	C
HC2	4110	39.0	44.2	1.13	C
HC3	4110	41.4	44.2	1.07	A
SERIES 3					
FA1	4850	125.4	182.8	1.46	C
FA2	4850	129.1	182.8	1.42	C
FA3	5000	129.5	185.5	1.43	C
SERIES 4					
FC1	4670	87.7	124.7	1.42	A
FC2	4670	84.8	124.7	1.47	A
SERIES 5					
FS1	5000	58.1	63.9	1.10	B
FS2	4660	56.1	60.6	1.08	B
FS3	4660	60.1	60.6	1.01	B

^aSee Table 8.

Table 8. Description of type of failures occurring in push-out test specimens

LETTER DESIGNATION	DESCRIPTION
A	Tensile cracking of the slab (simultaneous with concrete crushing adjacent to connector)
B	Fracture of the shear connector above the beam flange or weld preceded by cracking of the slab
C	Fracture in weld attaching the connector to the beam flange
D	Shearing of a wedge of concrete from under the connector (concurrent with the separation of the slab from the beam flange)

experimental values can be attributed to an unequal distribution of load between the two connectors caused by slight eccentricities of the specimen in the testing machine (21).

In Figure 17, the load-slip curves for half-scale, angle-plus-bar and channel shear connectors are presented. These load-slip curves (as well as others which follow) are the average of the load-slip curves for the individual specimens, which are presented in the Appendix. The angle-plus-bar connector provides more resistance to slip at all values of load. Compared to the half-scale channel, the angle-plus-bar connector provided a more rigid connection as well as a slightly higher ultimate strength.

The full-scale, angle-plus-bar shear connector (Series 3), which was previously used on composite bridges in Iowa, was compared to both channel connectors (Series 4) and the stud connectors (Series 5). Of the full-scale specimens tested, only Series 5 yielded results in good agreement with calculated values (ratios of predicted to experimental ultimate loads between 1.01 and 1.10). The low experimental results can again be attributed to slight eccentricity of the specimen in the testing machine. The results from the Series 3 and 4 specimens were in poor agreement with the calculated values (ratios between 1.42 and 1.47), although the low experimental ultimate load values, as well as failure modes, were very consistent within a given series.

The low results for the Series 4 specimens were probably caused by a large number of voids located adjacent to the loaded side of the

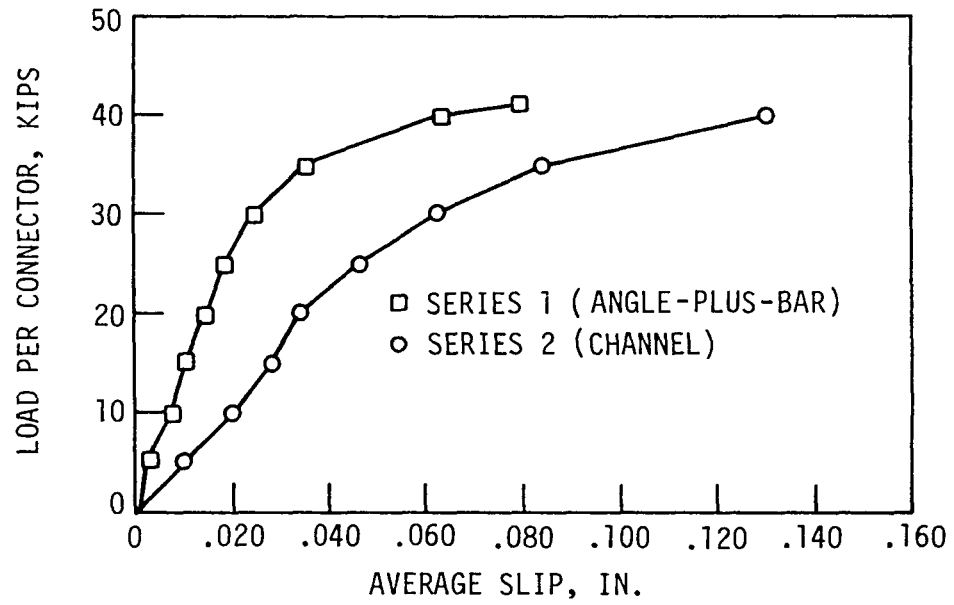


Fig. 17. Comparison of load-slip curves for half-scale connectors

connectors. After testing, when the slabs were fully separated from the connectors, it was discovered that voids comprised approximately 15% of the effective concrete bearing area. The percentage of voids found in the other specimens was found to be considerably less. A considerable number of the voids found were located near the channel flange welded to the beam. Previous research (21) has indicated that high stresses exist near the beam flange, and that the greatest portion of the load carried by a channel connector is carried by the flange welded to the beam. In Table 7, it can be noted that the Series 4 specimens (and one Series 2 specimen) failed by tensile cracking in the concrete slabs. Since this failure was a function of the dimensions of the slabs, this might also have caused the low experimental values.

Series 3 specimens also experienced failure at loads much lower than calculated. As can be noted in Table 7, all the Series 3 specimens failed through the weld. Inadvertently, a 3/16 in. weld was provided rather than the 1/4 in. weld specified on the bridge plans used for modeling the laboratory bridge (11). The shear and bending capacity of the 3/16 in. weld was calculated and found to be slightly below the observed ultimate load. By providing a 1/4 in. weld, the capacity would have been increased approximately 33%; thus, the ratio of predicted to experimental ultimate load would have been lowered considerably. In Section 4.1, it was noted that the separation of the slab from the beam, or "uplift," was considered a significant problem

on the Series 3 specimens. This is true because the angle-plus-bar connector, being a rigid connector, provides a greater resistance to slip, which increases the tendency of the slabs to separate from the beam. The failure of the weld at the leading (or first loaded) edge of the angle further influenced the separation tendency.

The load vs. slip curves for the full-scale shear connectors (Series 3, 4 and 5 specimens) are presented in Figure 18. For comparison, load-slip curves from two other research projects (15,21) are also given. As may be seen, the rigid, angle-plus-bar shear connectors provided more resistance to slip than the flexible channel or stud connectors. Referring back to Figure 17, this same difference in rigidity can be seen in the half-scale specimens (Series 1 and 2). As may be seen, there is good agreement between Series 5 and the previously tested studs (15). A lack of agreement at the lower loads can be attributed to the fact that the previously tested specimens were not pre-loaded (Series 5 specimens were pre-loaded to 10% of the ultimate) and some bond between the concrete and steel may have been present. The channel connector (Series 4) did not correlate very well with the previously tested channel connector (21). Though larger in size, as well as length, the Series 4 connector exhibited consistently lower values of load at equivalent values of slip. The presence of voids adjacent to the connector is thought to have caused the difference.

To summarize, a modified form of the AASHTO formula for the ultimate strength of a channel can be used to predict the capacity of

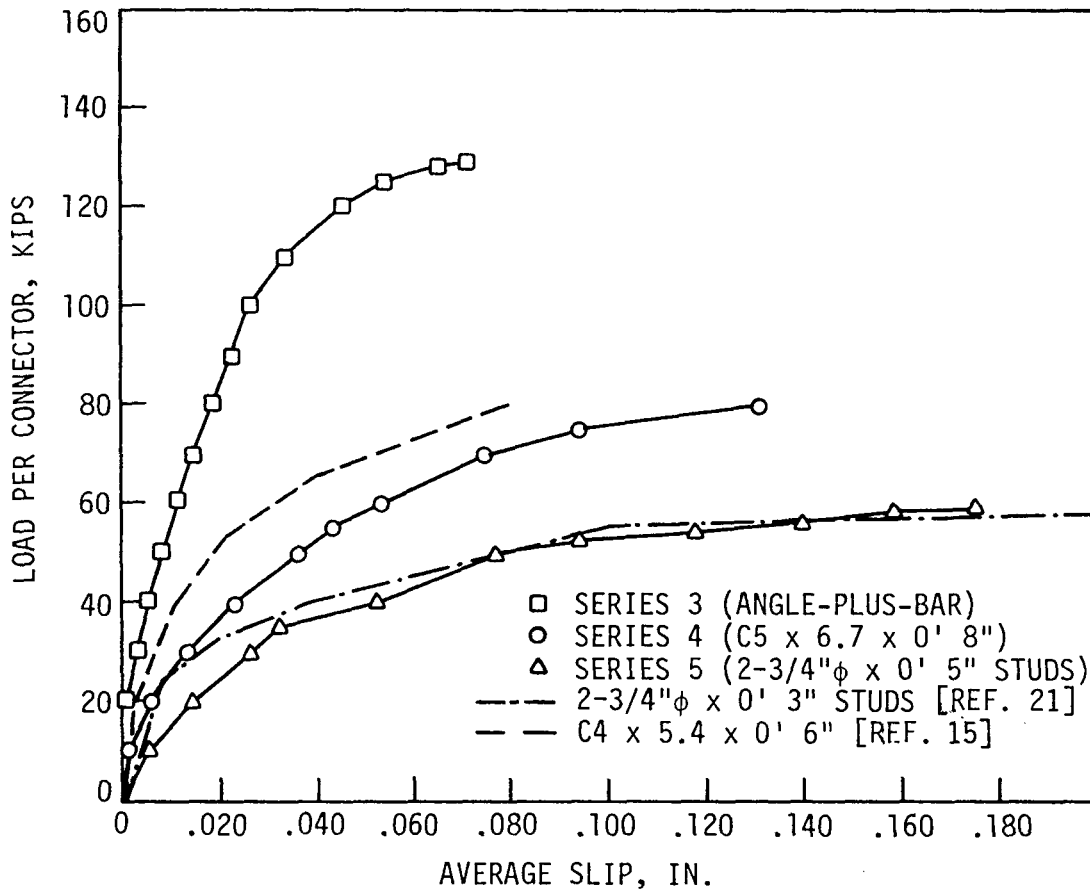


Fig. 18. Comparison of load-slip curves for full-scale connectors, Type A specimens

an angle-plus-bar shear connector. However, the weld capacity should be carefully checked for the effects of shear and bending. Keeping in mind that the push-out specimen provides a conservative estimate of shear connectors in a beam, the predicted ultimate load can be used safely for the static analysis of shear connectors on bridges already in use (18).

4.1.2 Type B Specimens

Type B specimens (Series 6 and 7), as stated in Section 1.2.1, were tested to discover the effectiveness of using high-strength bolts as shear connectors. The two bolt configurations tested (Figures 5 and 6) produced the results shown in Table 9. Although a limited number of specimens were tested, consistent results were obtained for each connector series. This agreement is evident in the ultimate load values in Table 9 and in the specimen load-slip curves which are presented in the Appendix.

In order to evaluate the effectiveness of Type B specimens, welded stud specimens (Series 5) were used for comparison. As may be observed in Figures 4, 5, and 6, the physical dimensions of the connectors were essentially identical (height was approximately 5 in. and the diameter was 3/4 in.). The main differences between the bolts and studs were the method of attachment to the beam flange (discussed in Section 2.1.2) and the tensile strength. The minimum tensile strength of a high-strength bolt is 120 ksi, while the tensile strength of a stud is approximately 71 ksi (15) or 40% less than the bolt.

Table 9. Push-out tests: Summary of test results and predicted ultimate loads for Type B specimens

SPECIMEN DESIGNATION	COMPRESSIVE STRENGTH, f'_c (PSI)		OBSERVED CONNECTOR ULTIMATE LOAD, KIPS	PREDICTED ^a ULTIMATE LOAD, KIPS	RATIO OF PREDICTED TO EXPERIMENTAL ULT. LOAD	TYPE ^b OF FAILURE
	SLAB	GROUT				
SERIES 6						
N1	5140	4550	65.4	65.3	1.00	B
N2	5140	4550	71.2	65.3	.917	B
N3	5140	4550	70.0	65.3	.933	B
N4	5140	4550	66.9	65.3	.976	B
SERIES 7						
E1	5180	5760	75.0	65.6	.875	B
E2	5180	5760	76.0	65.6	.863	B
E3	5180	5760	72.2	65.6	.909	B
E4	5180	5760	72.2	65.6	.909	B

^aPredicted ult. load based on AASHTO formula for welded studs (1).

^b See Table 8.

Comparing values from Tables 7 and 9, it is evident that the bolt connectors exhibited consistently higher values of ultimate load than the studs. The Series 6 specimens produced ratios of predicted to experimental ultimate load between .917 and 1.00 and the Series 7 ratios were between .863 and .909. Series 5 connector ratios were consistently greater than 1.01. The deviation in the ultimate strengths may be attributed to the large differences of tensile strength between the connectors, because an increase in the tensile strength is usually accompanied by an increase in shear strength. In Table 9, the ultimate load capacity of the epoxied bolt connector (Series 7) is shown to be slightly higher than the double-nut bolt connector (Series 6). This small difference is likely due to the reduced cross-sectional area on the double-nut bolts because the threads were located in the shear plane (Figure 5). Ratios of predicted to experimental ultimate load below 1.00 for the bolt connectors (Table 9) indicate that the AASHTO formula for the ultimate strength of studs provides a conservative estimate of the ultimate strength of high-strength bolt shear connectors.

As may be seen in Figure 19, there is good correlation between the Series 5, 6, and 7 specimen load-slip curves. Some of the variation at medium values of load were probably caused by the method of attachment to the beam (bolting versus welding). Up to loads of 15 to 20 kips, the curves have approximately the same slope. From 20 to 45 kips, the effect on the load-slip behavior due to bolting is noticeable. The lower resistance to slip of the bolts is probably related to the seating of the bolt in the hole through the flange. The seating effect was

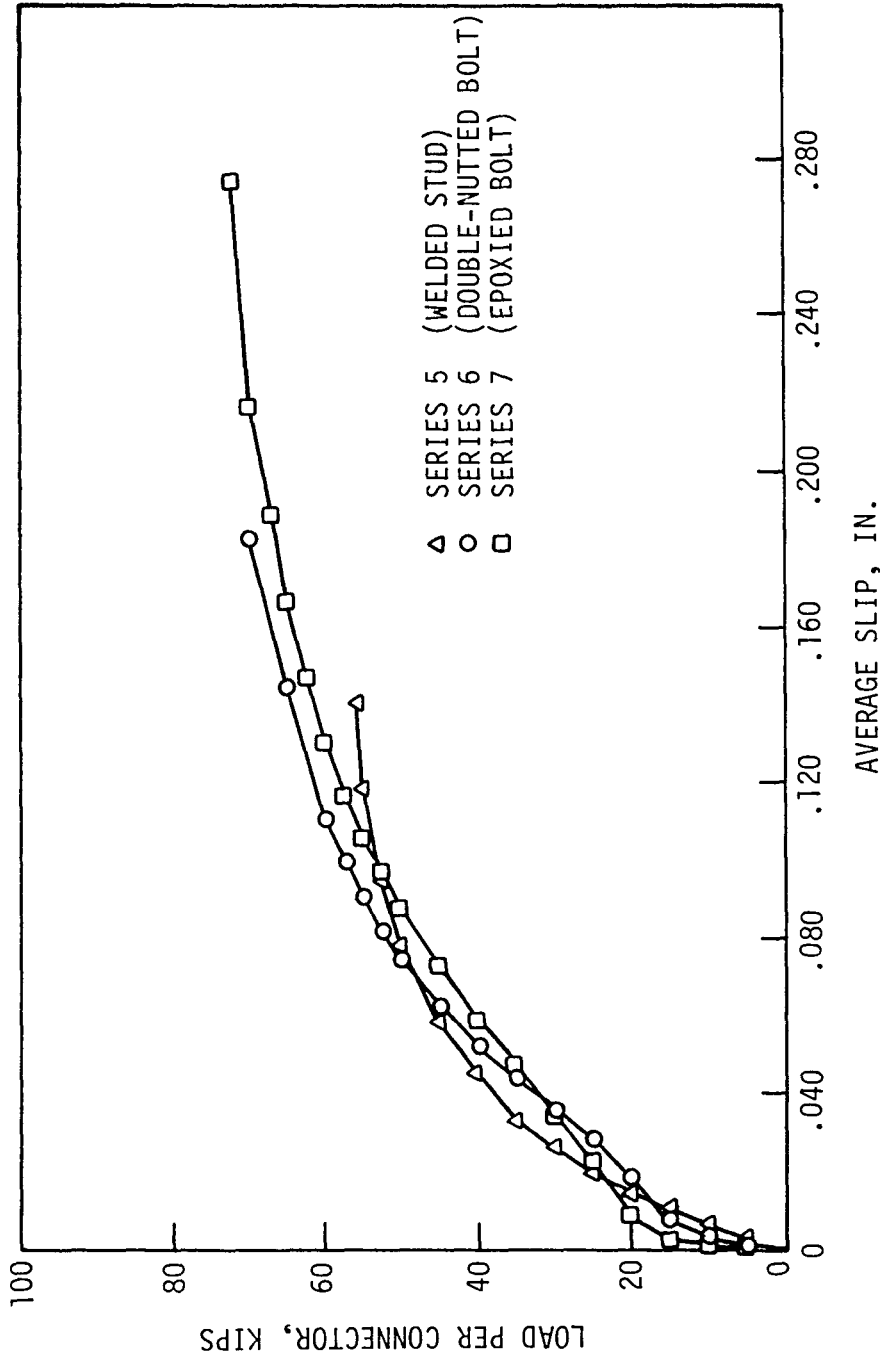


Fig. 19. Comparison of load-slip curves for Series 5, 6, and 7 specimens

caused by deformation of the bolt threads until bearing in the hole was achieved.

For loads up to 15 to 20 kips, the bolts provided a higher resistance to slip than the studs. This occurred in the Series 7 specimens, because the slab was clamped down to the beam by the bolt, and, thus, friction had to be overcome initially. The existence of the nut on the flange in the Series 6 specimens helped create a more rigid connection than that caused by a welded stud, because the nut provided a higher connector stiffness.

Variations in the load-slip characteristics between the double-nutted bolt connector (Series 6) and the epoxied bolt connector (Series 7) were minimal. Any differences can be explained by examining the methods of attachment to the beam flange. The bonding of the slab to the bolt, due to the epoxy and, more importantly, the frictional forces from pretensioning the bolt, probably helped to lower the initial slip values in the epoxied bolt connector. Beyond 30 kips, the double-nutted bolt connector was more resistant to slip. The main reason was the nut that was tightened against the beam flange. The nut provided more bearing area for the concrete and increased the connector stiffness adjacent to the beam. The location of high stresses at the base of the connector is a well-known fact (21,22). The addition of a nut at the base can be compared to increasing the flange thickness of a channel. The concrete restraint offered by increasing the bearing area tends to stiffen the connector which is directly

related to a decrease in slip at corresponding load levels (21). The double-nutted bolt connector is the easier to install. Referring to Section 2.1.2.2, it can be seen that the double-nut configuration can be implemented with fewer installation steps (only one coring operation and no epoxy to apply), quicker (metal shavings do not delay the procedure), and employing fewer materials and equipment (only one core bit needed and no epoxy is necessary). By using the AASHTO ultimate strength formula for studs (1), the ultimate strength of the double-nutted bolt connector can be conservatively estimated. The need for bolting rather than welding (due to unknown steel beam properties), coupled with the relative ease of application and conservative values of ultimate strength obtained through use of existing shear stud relationships, make the double-nut connector a viable method of increasing the shear capacity of existing composite beams. Previous studies (4,5) have shown that high-strength bolts performed satisfactorily under fatigue loading. Although a slightly different bolting technique was utilized, fatigue effects should not be significant in the author's opinion.

4.2 Composite Beam Test Results and Analysis

As previously mentioned in Section 1.2.2, the main thrust of these tests was to determine the effects of additional shear connectors on post-tensioned composite beams. Results and events of the elastic range tests will be presented in Section 4.2.1, and ultimate strength test results and occurrences will be discussed in Section 4.2.2.

By post-tensioning a composite beam, the post-tensioning tendons become part of the beam structure, thereby rendering the post-tensioned portion of the beam statically indeterminate to the first degree. When vertical load is applied to the beam, the force in the post-tensioning tendons will change (referred to as the Δ -T effect). The load-deflection relation for this system is nonlinear; however, for small values of post-tensioning, or axial, load (relative to the column buckling load) the relationship is essentially linear. Secondary P- Δ effects in the Δ -T analysis were neglected during Phase I. However, the large deflections caused by large vertical loads normally require the addition of P- Δ effects. Because the thrust of this testing was to discover the effects of variable amounts of shear connection, the P- Δ effects were ignored. Therefore, beams that were compared (e.g., Beams #1 and #4) had equal amounts of post-tensioning force applied. As will be seen, reasonable agreement between predicted and experimental ultimate moment values (Table 10) was obtained despite the omission of P- Δ effects.

4.2.1 Elastic Range Test Results and Analysis

Results presented and discussed in this section are for Tests A, B, and C, all of which involved loading which produced stresses in the steel beams below the elastic limit. Only experimental results are presented in the following paragraphs; comparisons between experimental results and theoretical results will be presented in the following section on ultimate strength. Tests A, B, and C were performed on all

Table 10. Summary of ultimate strength test results for the composite beam specimens

BEAM NO.	TYPE OF FAILURE	ULTIMATE VERTICAL LOAD, KIPS	ULTIMATE BENDING MOMENT, IN-KIPS				$\frac{M_u}{a}$
			M_u	M_u'	M_u''	M_u'''	
1	Shear connection	35.0	4140	3918	4529	4186 ^a	.989
2	Test stopped before failure	48.3	5813	5780	6529	6367 ^a	.913
3	Crushing of concrete slab	50.4	6102	5780	6534 ^a	N.A. ^b	.934
4	Crushing of slab and curb	38.1	4503	3918	4585 ^a	N.A. ^b	.982

M_u - experimental test moment (dead load included)

M_u' - theoretical based on no post-tensioning and adequate shear connection assumed

M_u'' - theoretical based on post-tensioning and adequate shear connection assumed

M_u''' - theoretical based on post-tensioning and inadequate shear connection

^aUse the theoretical bending moment as marked.

^bNot Applicable.

of the composite beams without any unusual occurrences.

Experimental midspan deflections, due to vertical load only, for the interior and exterior composite beams are presented in Figure 20 and Figure 21, respectively. As may be seen, there is very little difference in the resulting deflection behavior either due to the post-tensioning force (Test A, B, and C) or the additional shear connectors (Beam #1 vs. Beam #4 and Beam #2 vs. Beam #3). Deflections obtained from Test A (no prestress force locked in the beams) were most linear throughout the entire elastic range. This is expected because without the post-tensioning force applied the problem is linear. After the post-tensioning force is locked in, the relation between vertical load and deflection is nonlinear but, as shown in Figure 20 and Figure 21, this is insignificant throughout the entire elastic range.

The slight differences in deflections at lower values of load are most likely due to the varying degree of bond between the steel beam and concrete slab and variation of prestress force. Previous testing (during Phase I) when the beams were part of the half-scale model bridge as well as the cutting process, movement of the beams for testing, and the initial pre-load before each test accounted for the varying degree of bond present. Different values of prestress force also caused a slight variation in deflection (Figures 20 and 21). At higher values of prestress force, the composite beams tended to deflect more at lower values of vertical load. This is probably due to a lower moment of

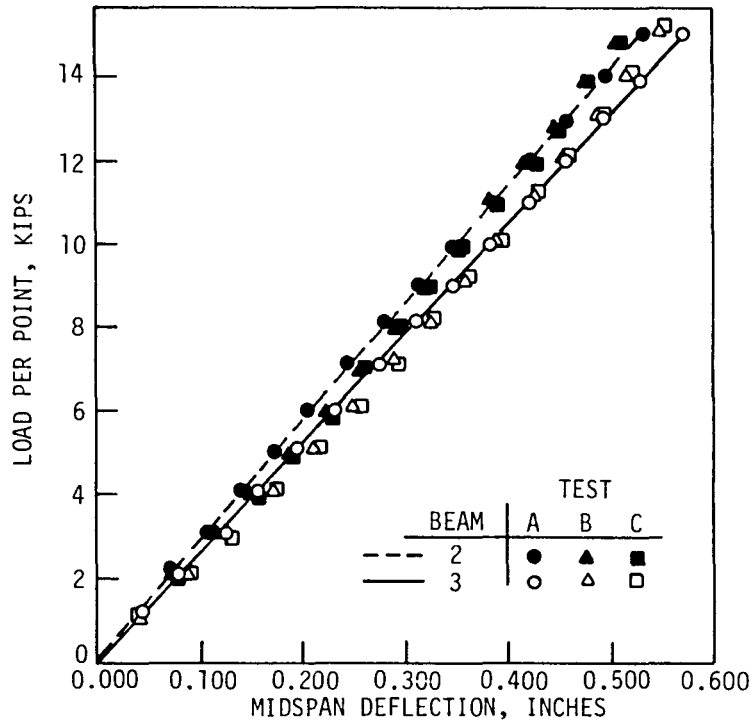


Fig. 20. Interior beam load-deflection curves for Tests A, B, and C

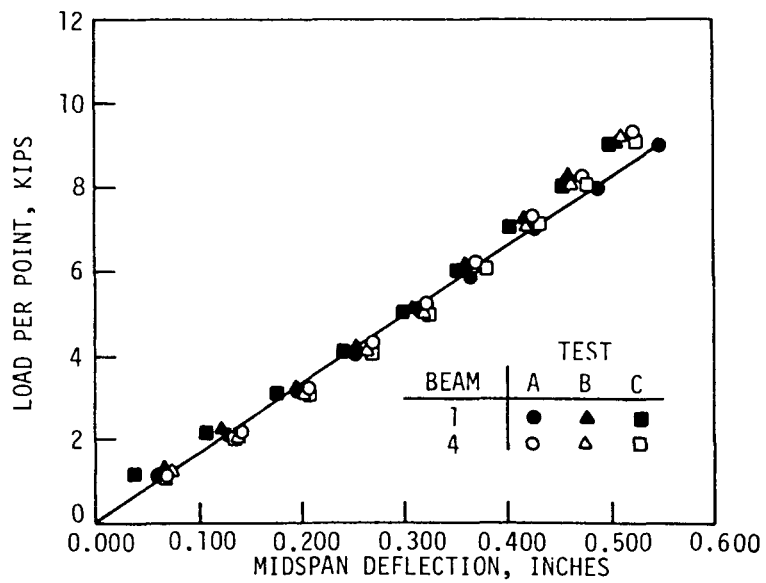


Fig. 21. Exterior beam load-deflection curves for Tests A, B, and C

inertia resulting from cracks in the concrete caused by prestressing. At higher values of vertical load, the concrete cracks were closed, thus increasing the stiffness of the post-tensioned composite beam.

Though both of the strengthened composite beams deflected slightly more than their unstrengthened counterparts, this was probably due to a small decrease in the moment of inertia because of a smaller slab width but mainly due to experimental error.

4.2.2 Ultimate Strength Test Results and Analysis

The ultimate strength test, Test D, performed on each composite beam provided data for vertical loading from 0 kips to ultimate. Data obtained from the various tests will be compared to illustrate the effects of varying the amount of shear connection in a post-tensioned composite beam. Theoretical results will also be compared to the experimental data.

Test 1D, performed on the "as fabricated" exterior composite beam (Beam #1), proceeded up to 18 kips per load point uneventfully. At a vertical load of 18 kips, deformation in the bracket and the flange under the bracket became visible. The beam continued to resist load; however, the rate of slip occurring increased more rapidly (as will be shown later). While loading proceeded, it was noted that the post-tensioning rods remained level as the beam deflected. Figure 22 shows bending in the rod at the bracket caused by the rods remaining level. This phenomenon was noted in all the composite beams when loaded to their ultimate strength.

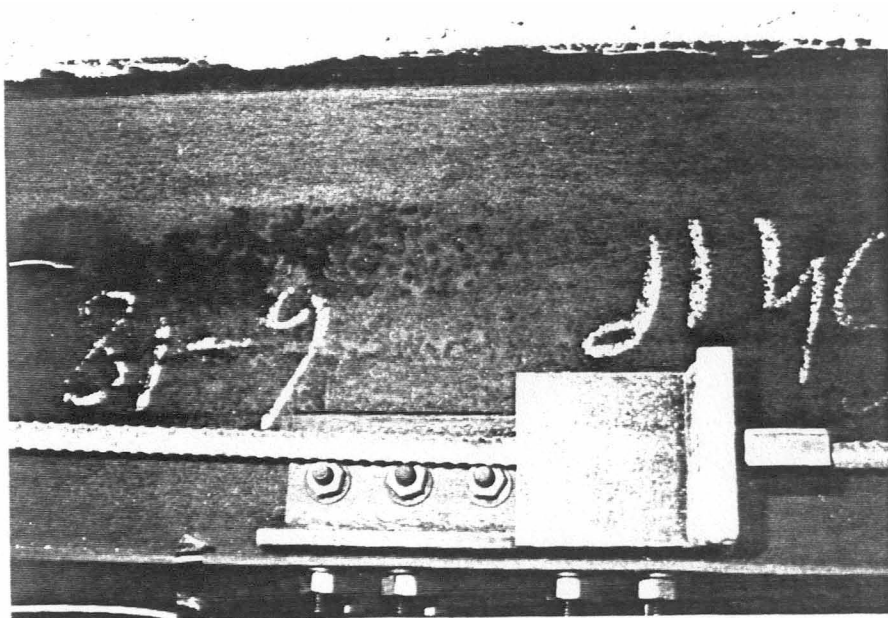


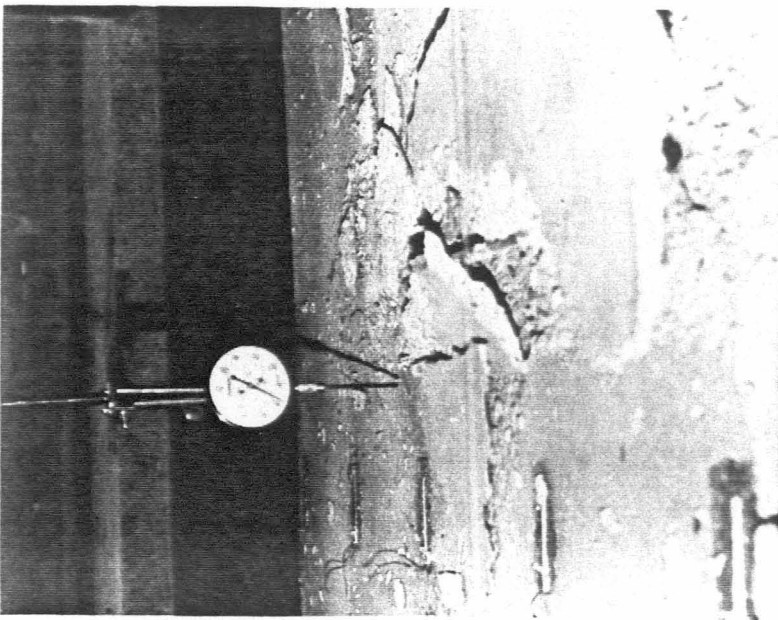
Fig. 22. Photograph of Beam #1 showing bending of the level post-tensioning rod at the bracket

At 30 kips, it was noticed that the bottom flange of the steel beam had rotated to within 1/16 in. of the abutment. At 35 kips, the sixth angle-plus-bar shear connector from one end failed. The composite beam failed to accept additional load at this point and testing was terminated. Upon closer examination, it was noted that the slab "rode up" over the shear connector. This phenomenon was similar to that found in the Series 1 push-out specimens. The maximum recorded end slip was .238 in. and the midspan displacement was approximately 3.57 in.

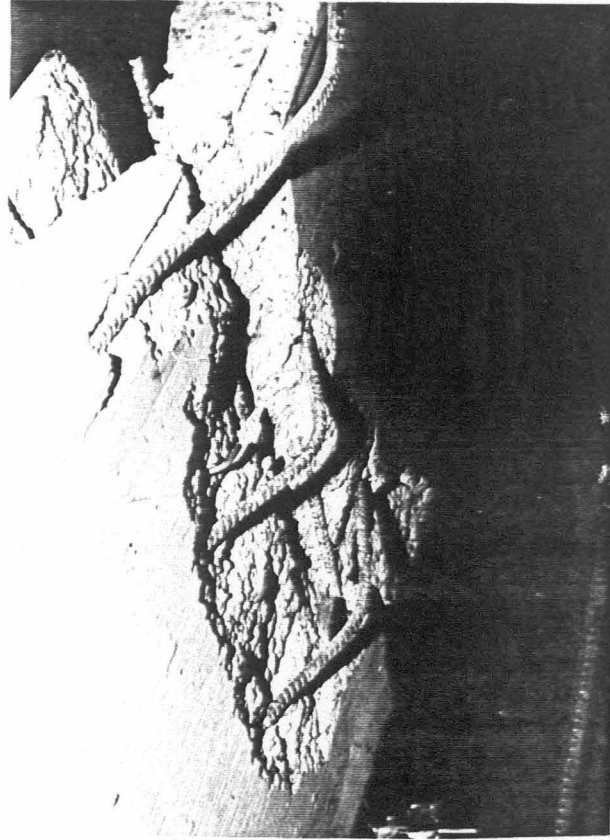
The other composite beam tested in the "as fabricated" condition, Beam #2, was loaded to a maximum of 48.3 kips per point. During Test 2D, the beam was noticed to have tilted slightly at a load of 18 kips as one centerspan deflection dial read 0.2" lower than the other. This value remained constant throughout the remainder of the test. The deflection dials were removed at 37 kips along with the other displacement gages to prevent damage if sudden failure occurred. A ruler at the midspan provided approximate displacement values and the end DCDTs measured relative slip until the test was terminated. At 48.3 kips, loading was stopped because of the danger of sudden failure in the testing frame. The maximum slip recorded was .015 in. and the midspan displacement was approximately 3 3/8 in. After the load was removed, permanent flange deformation of approximately 2 1/2 in. at midspan was observed. Some local buckling of the web under one load point (near the location where the diaphragms formerly framed in) was evident.

Test 3D, performed on the strengthened, interior composite beam (Beam #3), went according to plans up to a loading of 23 kips. At this point, flange deformation under the brackets was noticeable and the deflection dials were reset due to the large vertical deflections. Deflection dials and DCDTs, except those measuring slip, were removed at 44.2 kips (midspan displacement was 3.34 in.). Using a string line stretched between the beam ends and a ruler, midspan displacements were measured approximately. Testing was terminated at 48.8 kips because the usable stroke on the hydraulic jack was reached. At this point, cracks were observed on the underside of the slab, as well as crushing of the concrete on the top side of the slab at the span centerline; however, the beam was still capable of resisting load. At this point, the maximum midspan deflection and end slip was $5 \frac{9}{16}$ in. and .009 in., respectively.

In order to fail the composite beam, it was decided to release the load, add 3 in. of steel plate at the load points, and resume loading. Occasional readings were taken with a deflection dial and string line at midspan and two DCDTs to record end slip; all the measurements were initialized at 0 kips of vertical load. At a maximum load of 50.4 kips, a sudden compressive failure in the slab occurred at the span centerline. A top view of the slab crushing can be seen in Figure 23a and the bottom view is shown in Figure 23b. During reloading, the maximum deflection never exceeded $5 \frac{9}{16}$ in. and the final end slip was .009 in. The shear connectors showed no signs of distress;



a. Top of slab



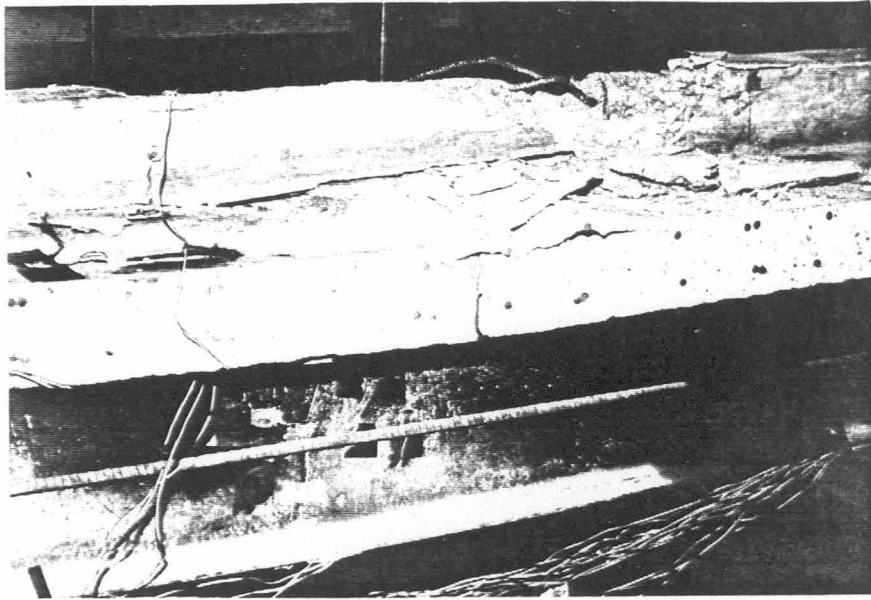
b. Bottom of slab

Fig. 23. Photographs showing concrete compressive failure in Beam #3

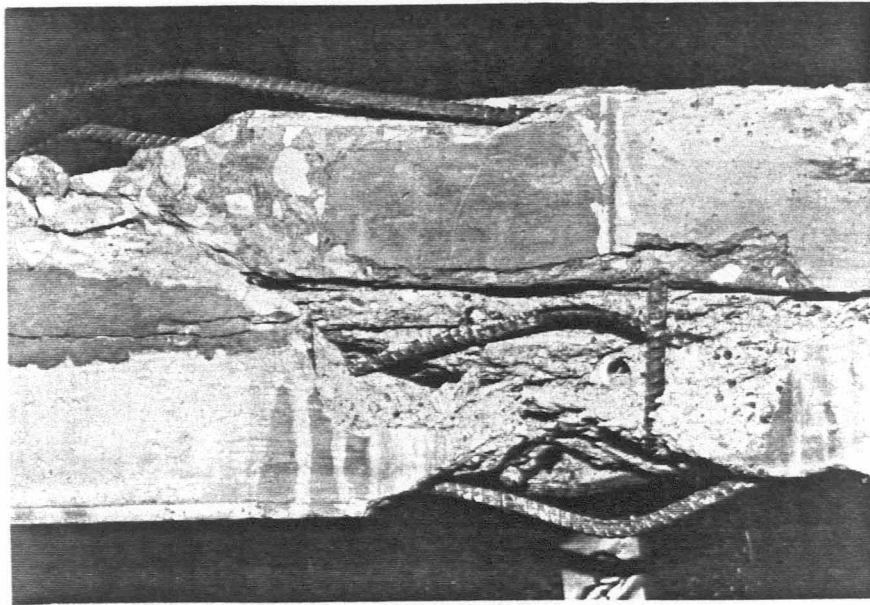
however, some web buckling was noted in the same location as in Beam #2.

The final ultimate strength test, Test 4D, proceeded uneventfully up to 22 kips where it was noted that the lower beam flange in the vicinity of the post-tensioning load brackets had deformed similar to the previous composite beams. At 24 kips, near one load point, concrete was visibly peeling away from the flange on the underside of the slab. The chipping of the concrete was noticeable later (at approximately 28 kips) under the other load point but eventually ceased at both locations around 30 kips. A loud cracking sound occurred at 33 kips and a sudden drop in load of 2 kips followed. Holding the load constant, it was discovered that the block of concrete under one of the jacks had cracked. It was decided to continue the test; just before the ultimate load of 38.1 kips was reached, a lateral bow of approximately 1/2 in. was observed. A sudden failure occurred simultaneously in the slab and curb 16 in. from the span centerline (Figure 24a). The compressive failure of the concrete was accompanied by local buckling of the top flange directly below the distressed concrete, as is shown in Figure 24b.

A comparison of theoretical and experimental ultimate bending moment values is presented in Table 10. As may be seen, the experimental moment was within 9.5% of the predicted capacity for all four composite beams. The predicted ultimate bending moments were based on a plastic stress distribution, which was modified when a state of inadequate



a. Curb and slab failure

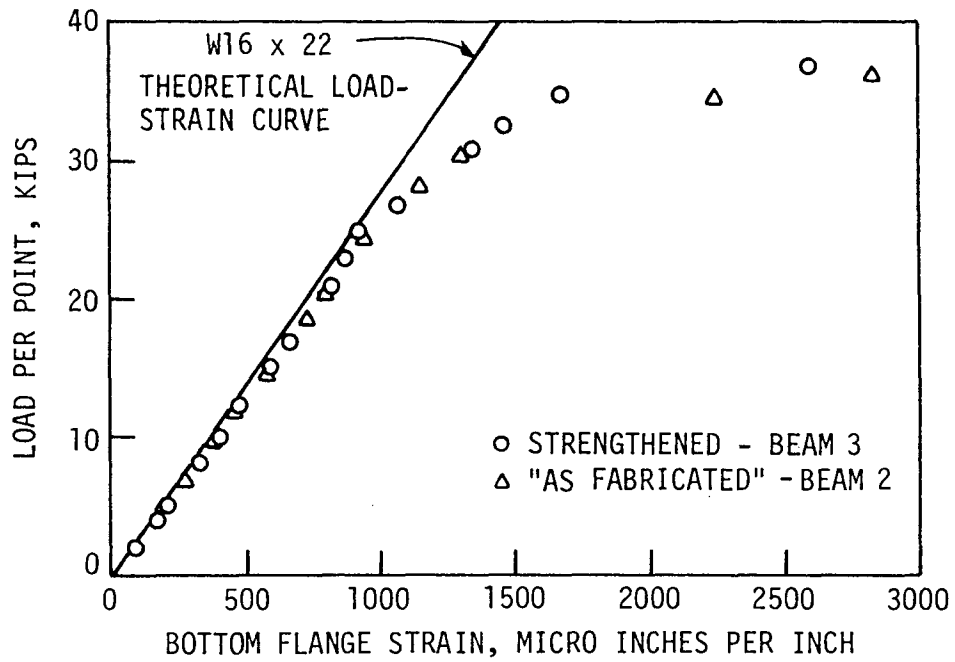


b. Top flange failure

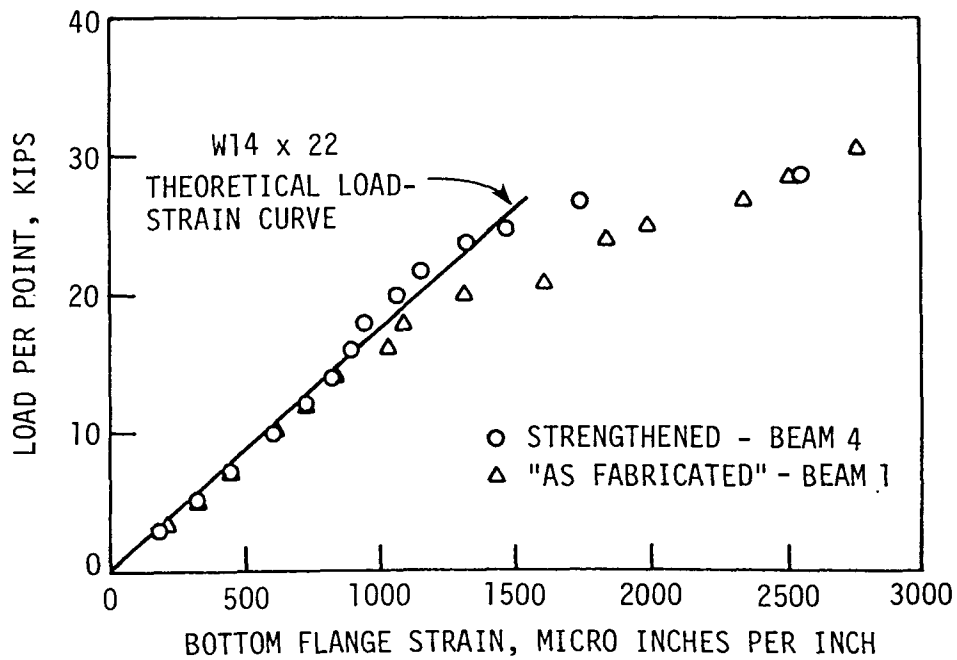
Fig. 24. Photographs of the failure mechanism in Beam #4

shear connection existed (18). The exterior-type composite beams, Beams #1 and #4, provided experimental values that agreed very well with the predicted values (Table 10). Also, it should be noted that the addition of shear connectors increased the experimental ultimate moment capacity only 8.8%. If the effects of post-tensioning aren't included, the theoretical ultimate moment capacity of the exterior and interior beams is reduced approximately 14% and 11.5%, respectively. The type of failure, given in Table 10, for all of the composite beams was as predicted. Beams #3 and #4, provided with an adequate shear connection, failed by slab (and curb) crushing, while Beam #1, with inadequate shear connection, failed through the shear connection. Beams #2 and #3, interior-type beams, also provided reasonable results. Though Test 2D was terminated, the maximum experimental moment was close to the predicted value. The experimental moment obtained in Test 3D could have been the result of stopping the test to extend the stroke on the hydraulic jack before testing to failure. Some crushing of the concrete was noted before stopping the test and the reduction in cross-sectional area of the slab probably reduced the ultimate moment slightly.

Figure 25 presents the effects of different levels of shear connection on the bottom flange strains. As may be seen, there was small variation due to the amount of shear connection, especially at low loads. This agrees with the fact that the difference in relative slip between "as fabricated" and strengthened beams was very small (as will be seen in Figure 28). Reasonable correlation between experimental



a. Comparison of interior beams and theory



b. Comparison of exterior beams and theory

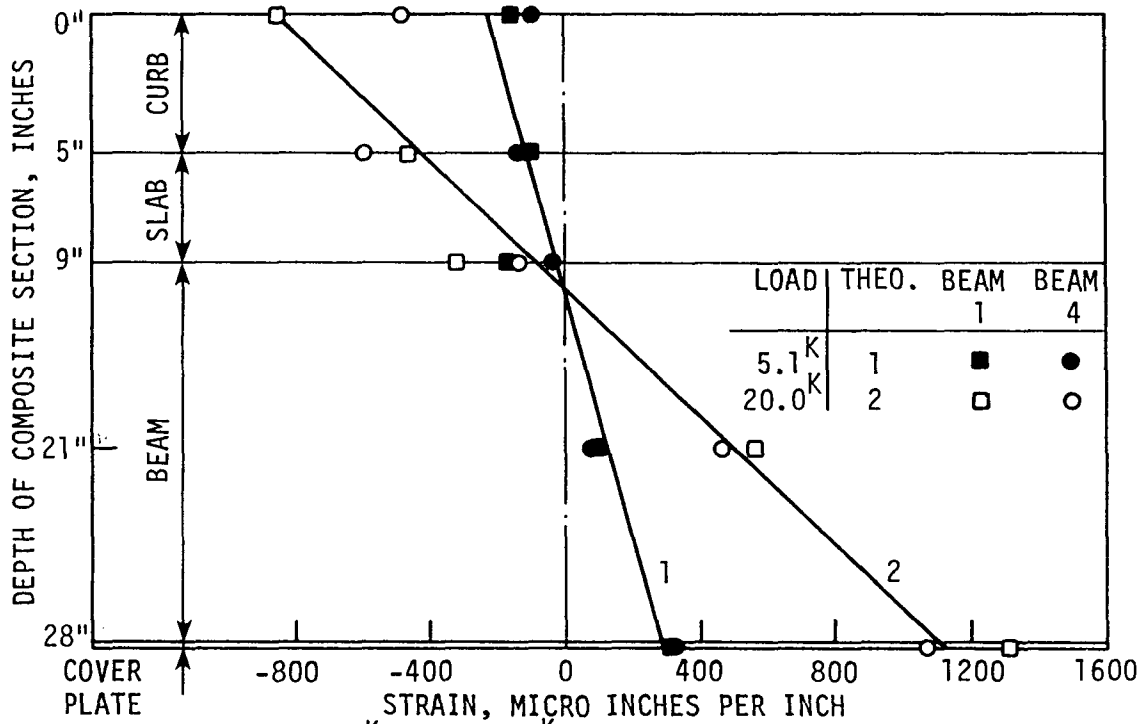
Fig. 25. Load-midspan strain curves for composite beams

and computed strains is also shown in Figure 25. The theoretical strains were based on full interaction between the beam and slab.

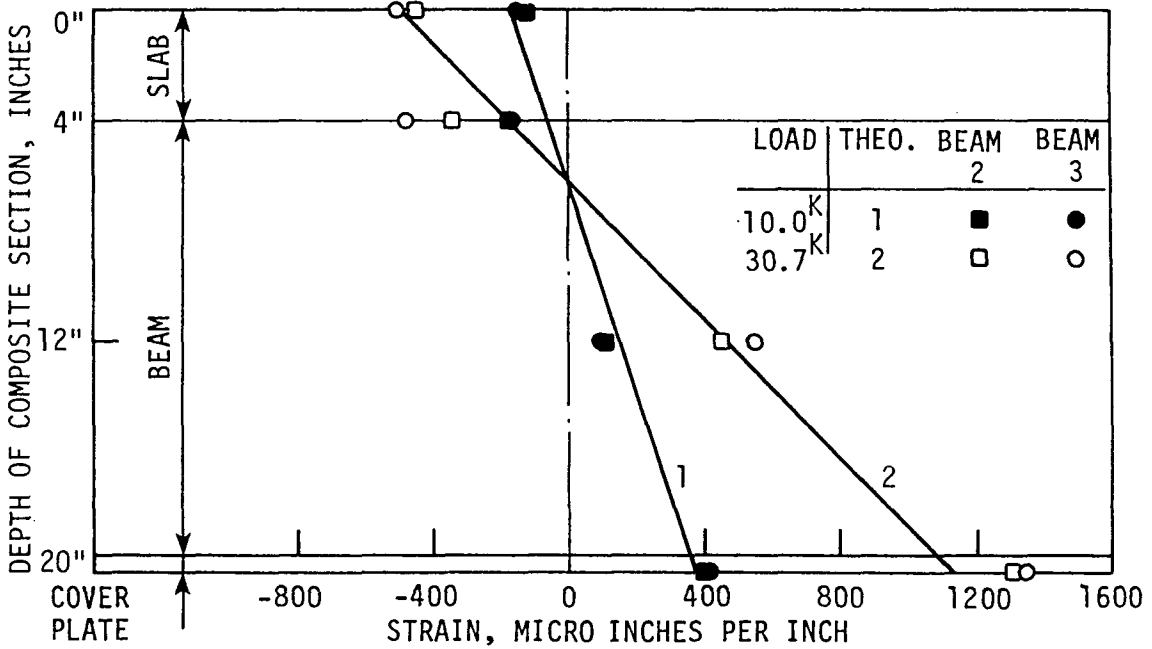
Profiles of strain at the centerline are given in Figure 26 for the various beams at several levels of loading. Once again the observed strains agree well with calculated strains (based on full interaction), as well as between beams with different amounts of shear connection. The strains at the higher values of load did not correlate as well with the theoretical strain profiles. These differences were most noticeable at the steel-concrete interface where slip may occur, thus creating a localized effect at the gages.

In all tests, the measured deflection exceeded the theoretical bending deflections, as illustrated in Figure 27. The theoretical deflections are based on 100% interaction between the concrete and steel beam and on the steel beam acting alone. As shown in Figure 27, the experimental values are closer to the 100% interaction line. This high degree of interaction agrees with the low relative slips experimentally obtained. The theoretical curves in Figure 27 are based on deflections due to bending effects only (no shear deformation effects or $P-\Delta$ effects) and, therefore, underestimate the observed deflections.

Illustrated in Figure 28 are the load vs. end slip curves for each of the composite beams. As may be seen, the difference in slip between the strengthened and "as fabricated" beams at low loads is small. The rigid nature of the angle-plus-bar connectors result in low values of slip which may lower the difference in slips, especially



a. $P = 5.1^K, P = 20.0^K$ for exterior-type beams



b. $P = 10.0^K, P = 30.7^K$ for interior-type beams

Fig. 26. Midspan strain profiles at various values of load per point

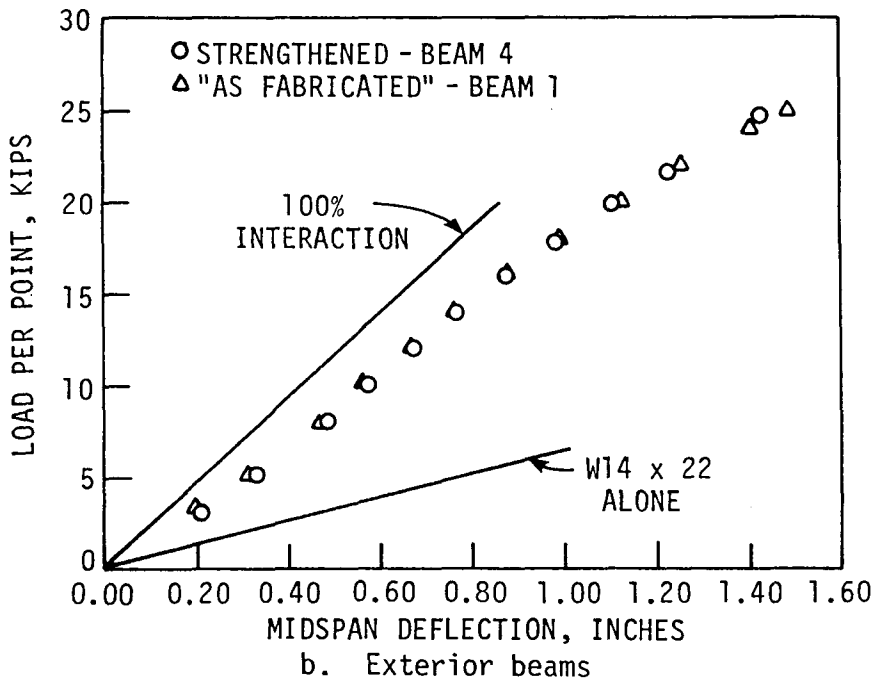
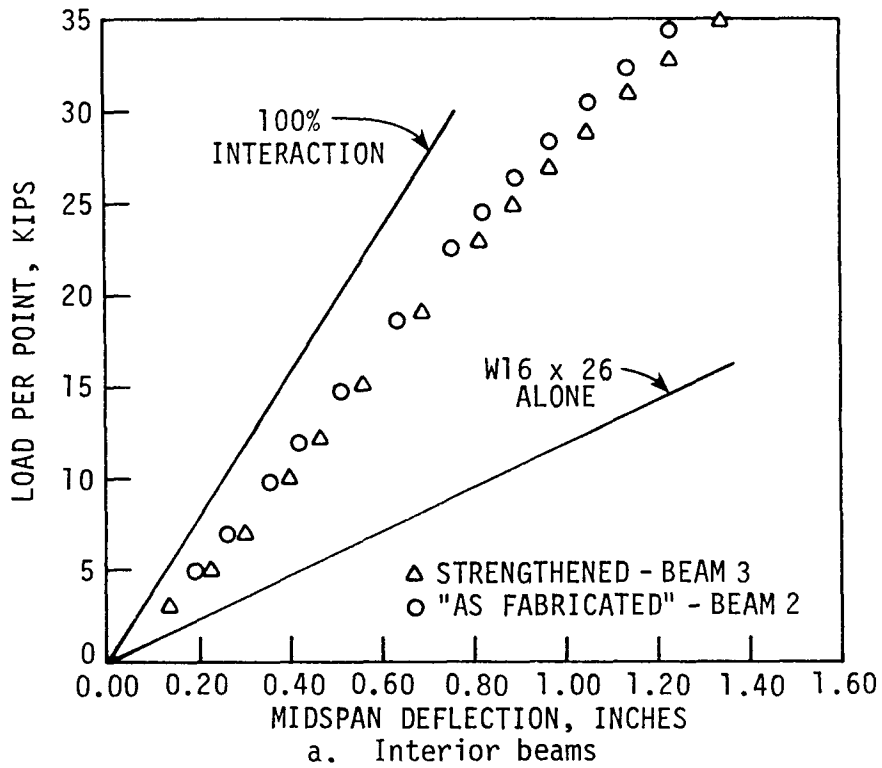


Fig. 27. Comparison of theoretical and experimental load-deflection curves

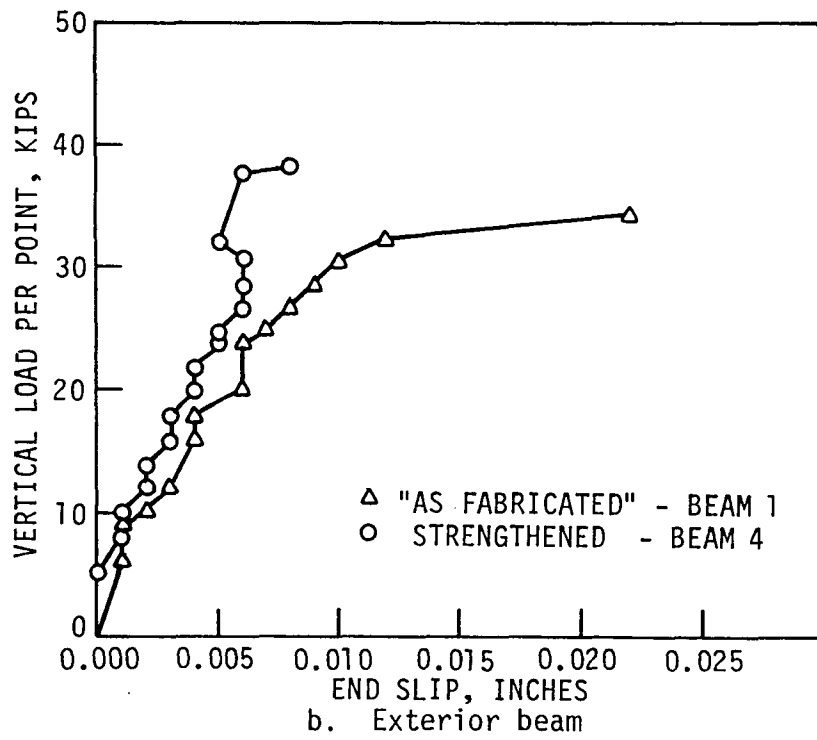
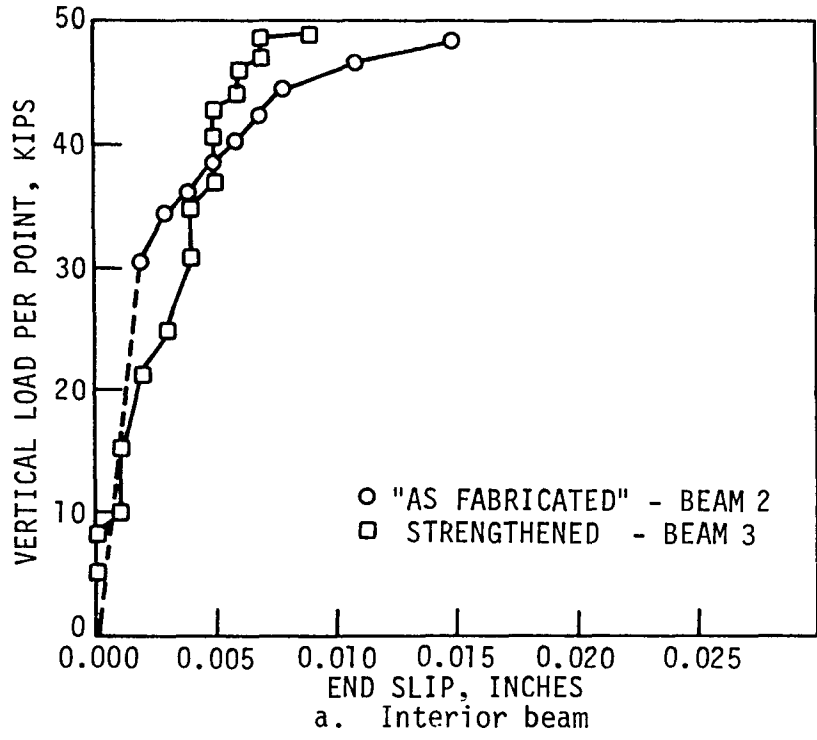


Fig. 28. Load-end slip curves

at small values of load. At approximately 70% of the ultimate load, the "as fabricated" beams tended to exhibit more slip as a result of having less shear connectors. Though Beam #2 was not taken to failure, it can be noted that the increase in the slip was increasing at approximately the same rate as Beam #1, which failed through the shear connectors.

Figure 29 presents the experimental force per connector vs. relative slip for each of the composite beams and the average load-slip curve for the Series 1 push-out specimens. The approximate force in the shear connector was found by expressing the vertical load in terms of horizontal shearing force. Because Beams #3 and #4 had two different types of shear connectors (angle-plus-bar and high-strength double-nutted bolt), a value for the bolt connectors in terms of the angle-plus-bar was approximated. As shown in Figure 29, a typical connector in each of the composite beams provided roughly the same amount of resistance to slip at equal values of force. The load vs. slip curves from the composite beams were of the same shape as the Series 1 curve, even though the values of slip were much lower. As previously noted for the same connector, results from push-out tests are more conservative than composite beam results. It may also be noted in Figure 29 that the connector in Beam #1 has a maximum calculated force of 39.9 kips, which is similar to that found experimentally by the push-out tests (6% higher). All other beams had connector forces lower than the push-out test connectors. This agrees

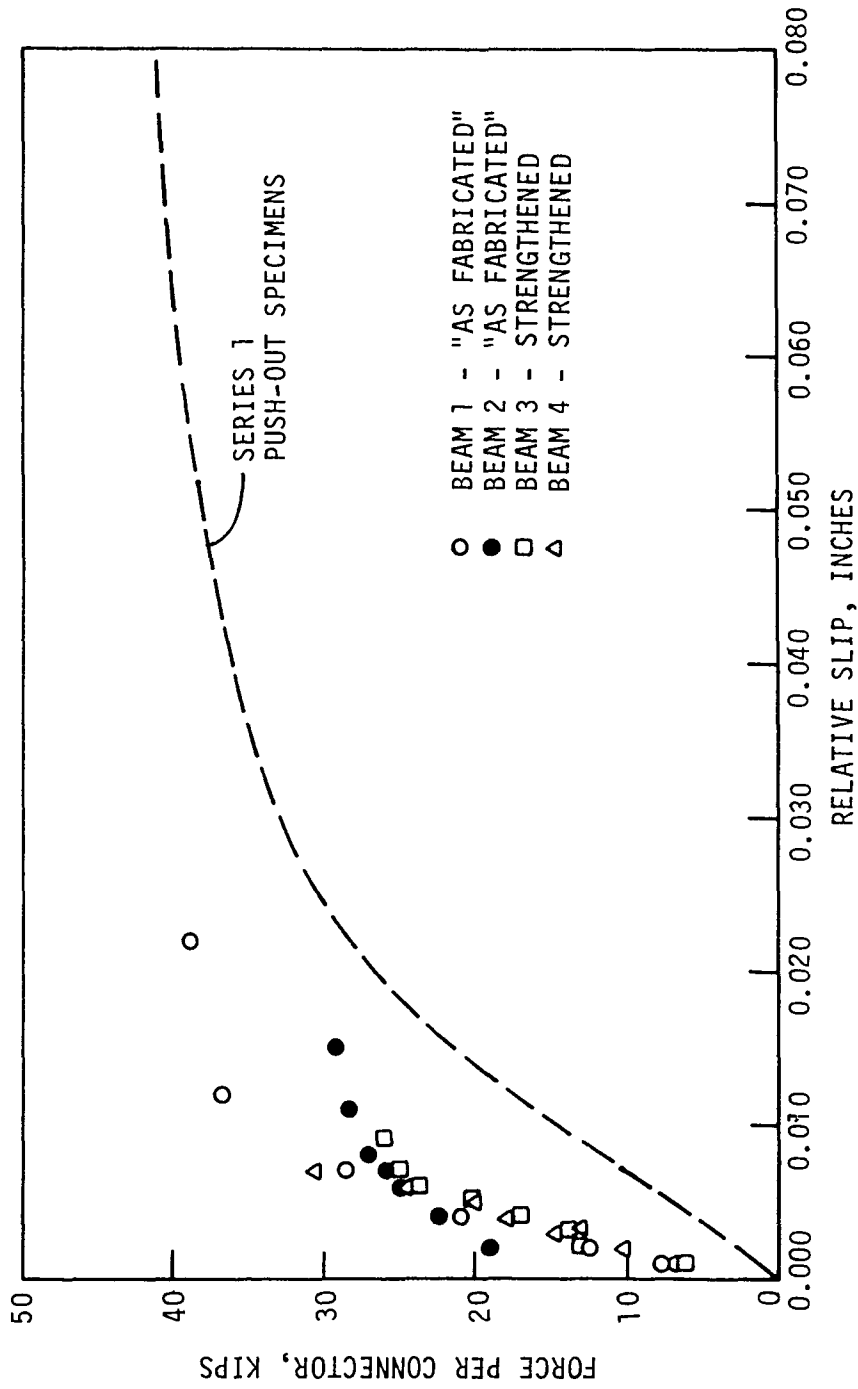


Fig. 29. Load-slip curves for each composite beam

with the fact that only Beam #1 failed in its shear connection, while the other beams (except Beam #2) failed by crushing of the concrete.

5. SUMMARY AND CONCLUSIONS

5.1 Summary

The rehabilitation of composite bridges by post-tensioning the steel beams was investigated in an earlier study (11). This study was undertaken to investigate the inadequate shear connection that exists between the deck and steel beams as a result of changes in design philosophies.

The literature review substantiated the use of push-out tests to determine the strength of shear connectors. Previous research had indicated that high-strength steel bolts might be substituted for welded stud connectors of the same diameter, with a gain in ultimate capacity and no loss of fatigue capacity.

This study summarizes the results of the laboratory testing of 22 two slab push-out specimens and 4 composite concrete slab-steel beam specimens. The composite beam specimens were cut from the model bridge utilized in Phase I (11).

Good correlation was found between the experimental results of the push-out tests and the theoretical results. Also, there was excellent agreement in the ultimate strengths and load-slip characteristics of the specimens in a given series.

The ultimate strength of angle-plus-bar shear connectors, employed on existing bridges, was found theoretically with a modified form of the AASHTO formula for the ultimate strength of channel

shear connectors. Good agreement between experimental and theoretical results was found, but it was noted that care must be taken not to exceed the capacity of the weld between the angle and wide flange beam. This is due to the rigid nature of the angle-plus-bar connector which increases the separation between the slab and beam, thereby increasing the bending stresses on the connector weld.

Two methods of increasing the shear capacity of composite bridges without welding, as the type of steel in some bridges is unknown, were tested; both involved high-strength bolts as shear connectors. The ultimate capacity of the high-strength bolts was conservatively predicted using the AASHTO formula for the ultimate strength of welded stud shear connectors. Experimentally obtained values were consistently higher than predicted values, while the load-slip characteristics of the bolt connectors were very similar to the stud connectors. On the basis of its behavior and ease of installation, the double-nutted bolt shear connector was used to strengthen two of the composite beams.

The shear capacity of the four composite beams was predicted, employing the results of the push-out tests. Because the shear capacity was inadequate to develop the full bending capacity of the composite beams, double-nutted shear connectors were added to two of the beams employing the procedure used for the push-out specimens.

Deformation of the beams near the post-tensioning brackets and of the post-tensioning tendon at the brackets occurred, but the

post-tensioning system did not fracture. Instead, beam failures were the result of shear connector failure or crushing of the slab (and/or curb) concrete. Ultimate moment capacity was closely predicted (within 10% of experimental values) for each of the beams utilizing a plastic stress distribution. To account for a state of inadequate shear connection, the plastic stress distribution was modified.

The addition of shear connectors affected the load-slip characteristics at large values of vertical load and increased the ultimate moment capacity slightly, however, the load-deflection curves weren't significantly affected. Adding shear connectors also prevented failure of the shear connection, in the case of the exterior beams. The force developed in the composite beam shear connectors was similar to that developed by the connectors in the push-out specimens.

Strains and deflections were predicted fairly accurately when based on full interaction of the slab and steel beam. Experimentally obtained deflections were consistently higher than those predicted with full interaction.

Post-tensioning had little noticeable effect on the load-slip or load-deflection characteristics of the composite beams, when loaded in the elastic range of the steel beam. Secondary post-tensioning effects ($P-\Delta$ and $\Delta-T$) were ignored in the theoretical analysis of the beams, but the accuracy of the predicted ultimate moment values were unchanged. Computation of the ultimate moment capacity without the effects of post-tensioning indicates a reduction up to 14% of the beam capacity.

5.2 Conclusions

1. The ultimate shear strength of angle-plus-bar shear connectors can be approximated using a modified form of the AASHTO formula for the ultimate strength of channels. It is extremely important to consider the strength of the weld used to attach the connector to the beam flange.
2. High-strength bolts can be used as shear connectors with little or no difference in the strength or behavior from that of welded shear studs.
3. High-strength bolts attain a higher ultimate strength than welded studs. A conservative value of ultimate shear strength can be obtained employing the AASHTO formula for welded stud ultimate strength.
4. Based on the limited number of tests performed, the shear capacity of a composite beam can be increased by the addition of double-nutted high-strength bolt connectors.
5. The ultimate moment capacity of a composite beam can be slightly increased by the addition of bolt connectors in this particular configuration.

6. ACKNOWLEDGMENTS

The work described in this thesis was conducted at the Iowa State University structures laboratory, Ames, Iowa, by the Engineering Research Institute of Iowa State University and made possible by funding from the Iowa Department of Transportation under Research Project HR 238.

I wish to express my appreciation to Dr. Wayne Klaiber for his support and guidance during the preparation of this thesis. Appreciation is also extended to Dr. W. W. Sanders, Jr. and Kenneth Dunker for their assistance in the conduct of this project. I thank Dr. Lowell Greimann and Dr. Fred Graham for sitting on my committee.

Special thanks are given to Doug Wood, Research Associate, for his assistance in various phases of the project. Thanks are also due to the undergraduate students, Tim Dedic and Brad Beck, for their contributions to this investigation.

I am especially grateful to my wife, Margaret, for her continued understanding and encouragement throughout this project.

7. REFERENCES

1. American Association of State Highway and Transportation Officials. Standard Specifications for Highway Bridges. 12th edition. Washington, D.C.: American Association of State Highway and Transportation Officials, 1977.
2. Cook, J. P. Composite Construction Methods. New York: John Wiley and Sons, Inc., 1977.
3. Dallam, L. N. "Pushout Tests With High-Strength Bolt Shear Connectors." Missouri Cooperative Highway Research Program Report 68-7. Engineering Experiment Station, University of Missouri-Columbia, 1968.
4. Dallam, L. N. "Static and Fatigue Properties of High-Strength Bolt Shear Connectors." Missouri Cooperative Highway Research Program Report 70-2. Engineering Experiment Station, University of Missouri-Columbia, 1970.
5. Dorton, R. A., M. Holowka, and J. P. C. King. "The Conestoga River Bridge - Design and Testing." Canadian Journal of Civil Engineering, 4, No. 1, March, 1977.
6. Gaylord, E. H., Jr., and C. N. Gaylord, Editors. Structural Engineering Handbook. Second edition. New York: McGraw-Hill Book Company, 1979.
7. Goble, G. G. "Shear Strength of Thin Flange Composite Specimens." American Institute of Steel Construction, Engineering Journal, 5, No. 2 (April, 1968), 62-65.
8. Heins, C. P., and D. A. Firmage. Design of Modern Steel Highway Bridges. New York: John Wiley and Sons, Inc., 1979.
9. Johnson, R. P. Composite Structures of Steel and Concrete. Vol. 1. New York: John Wiley and Sons, Inc., 1975.
10. Klaiber, F. W., K. F. Dunker, and W. W. Sanders, Jr. "Strengthening of Single Span Steel Beam Bridges." Journal of the Structural Division, Proceedings, ASCE, 108, No. ST12 (December, 1982), 2766-2780.
11. Klaiber, F. W., K. F. Dunker, and W. W. Sanders, Jr. "Feasibility Study of Strengthening Existing Single Span Steel Beam Concrete Deck Bridges." Final Report. Engineering Research Institute, Iowa State University, Ames, Iowa, 1981.

12. Klaiber, F. W., W. W. Sanders, Jr., and D. J. Dedic. "Post-Tension Strengthening of Composite Bridges." Final Report. IABSE Symposium on Maintenance, Repair, and Rehabilitation of Bridges, 39, International Association of Bridge and Structural Engineers, 1982, 123-128.
13. Knowles, P. R. Composite Steel and Concrete Construction. New York: John Wiley and Sons, Inc., 1973.
14. Ollgard, J. G. "The Strength of Stud Shear Connectors in Normal and Lightweight Concrete." M.S. Thesis. Lehigh University, Bethlehem, Pennsylvania, 1970.
15. Ollgard, J. G., R. G. Slutter, and J. W. Fisher. "Shear Strength of Stud Connectors in Lightweight and Normal-Weight Concrete." American Institute of Steel Construction, Engineering Journal, 8, No. 2 (April, 1971), 55-64.
16. Sabnis, G. M., Editor. Handbook of Composite Construction Engineering. New York: Van Nostrand Reinhold Company, 1979.
17. Siess, C. P., N. M. Newmark, and I. M. Viest. "Small Scale Tests of Shear Connectors and Composite T-Beams." Studies of Slab and Beam Highway Bridges: Part III. University of Illinois Bulletin, 49, No. 45, Bulletin Series No. 396 (February, 1952).
18. Slutter, R. G., and G. C. Driscoll. "Flexural Strength of Steel-Concrete Beams." Journal of the Structural Division. Proceedings, ASCE, 91, No. ST2 (April, 1965), 71-99.
19. Viest, I. M. "Investigation of Stud Shear Connectors for Composite Concrete and Steel T-Beams." Journal of the American Concrete Institute, 27, No. 8 (April, 1956), 875-891.
20. Viest, I. M., and C. P. Siess. "Design of Channel Shear Connectors for Composite I-Beam Bridges." Public Roads, 28, No. 1 (April, 1954), 9-16.
21. Viest, I. M., C. P. Siess, J. P. Appleton, and N. M. Newmark. "Full Scale Tests of Channel Shear Connectors and Composite T-Beams." Studies of Slab and Beam Highway Bridges: Part IV. University of Illinois Bulletin, 50, No. 29, Bulletin Series No. 405 (December, 1952).
22. Yam, L. C. P. Design of Composite Steel-Concrete Structures. London: Surrey University Press, 1981.

8. APPENDIX. LOAD-SLIP AND LOAD-SEPARATION CURVES

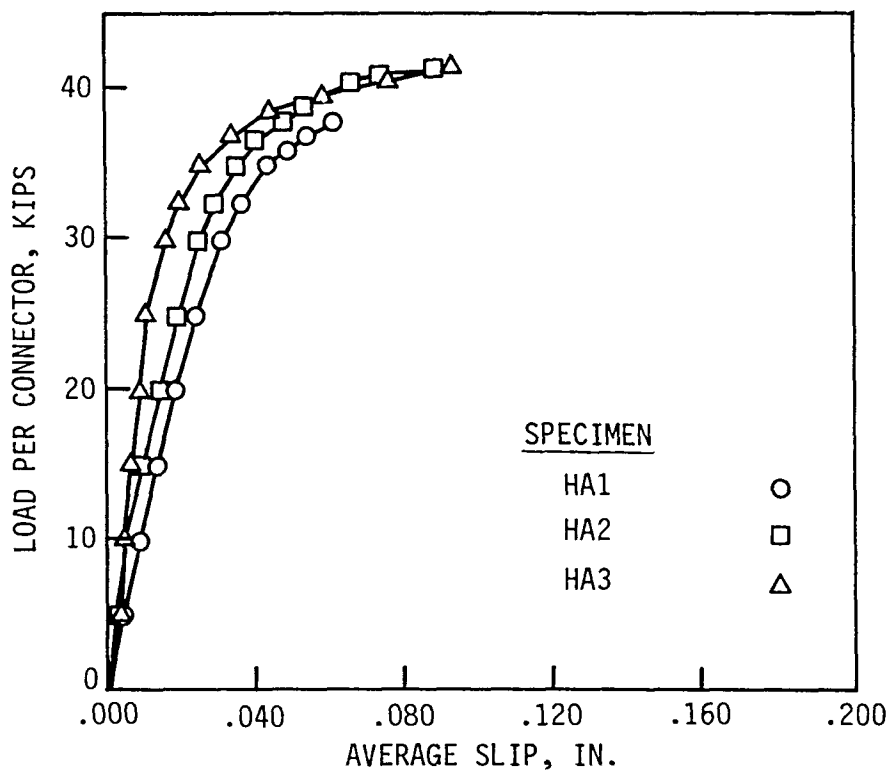


Fig. A.1. Load-slip curves for individual Series 1 push-out specimens

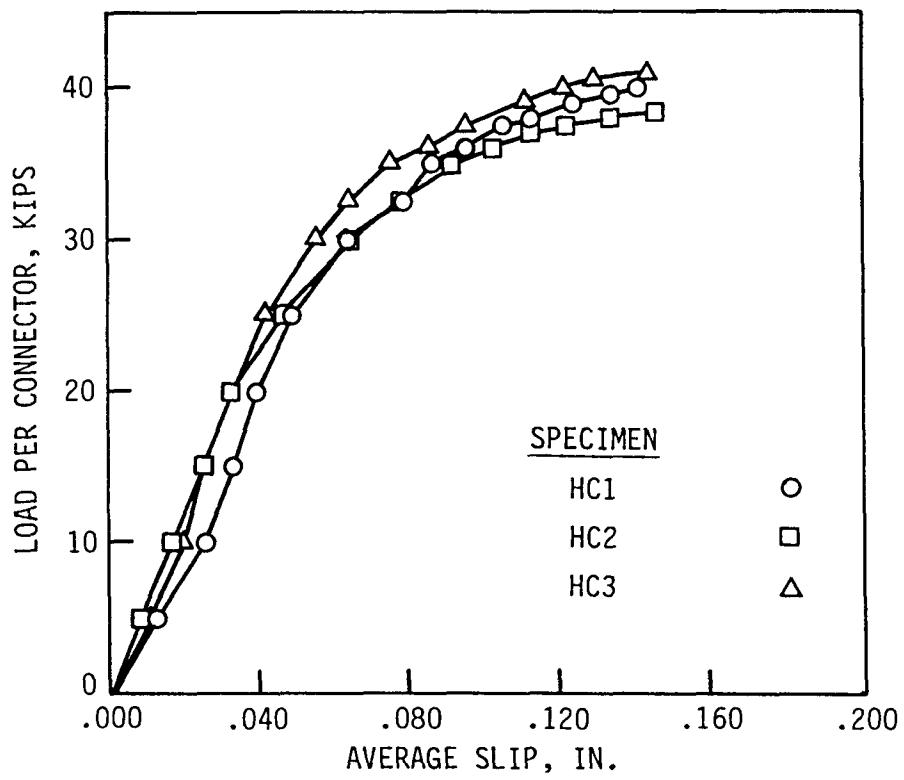


Fig. A.2. Load-slip curves for individual Series 2 push-out specimens

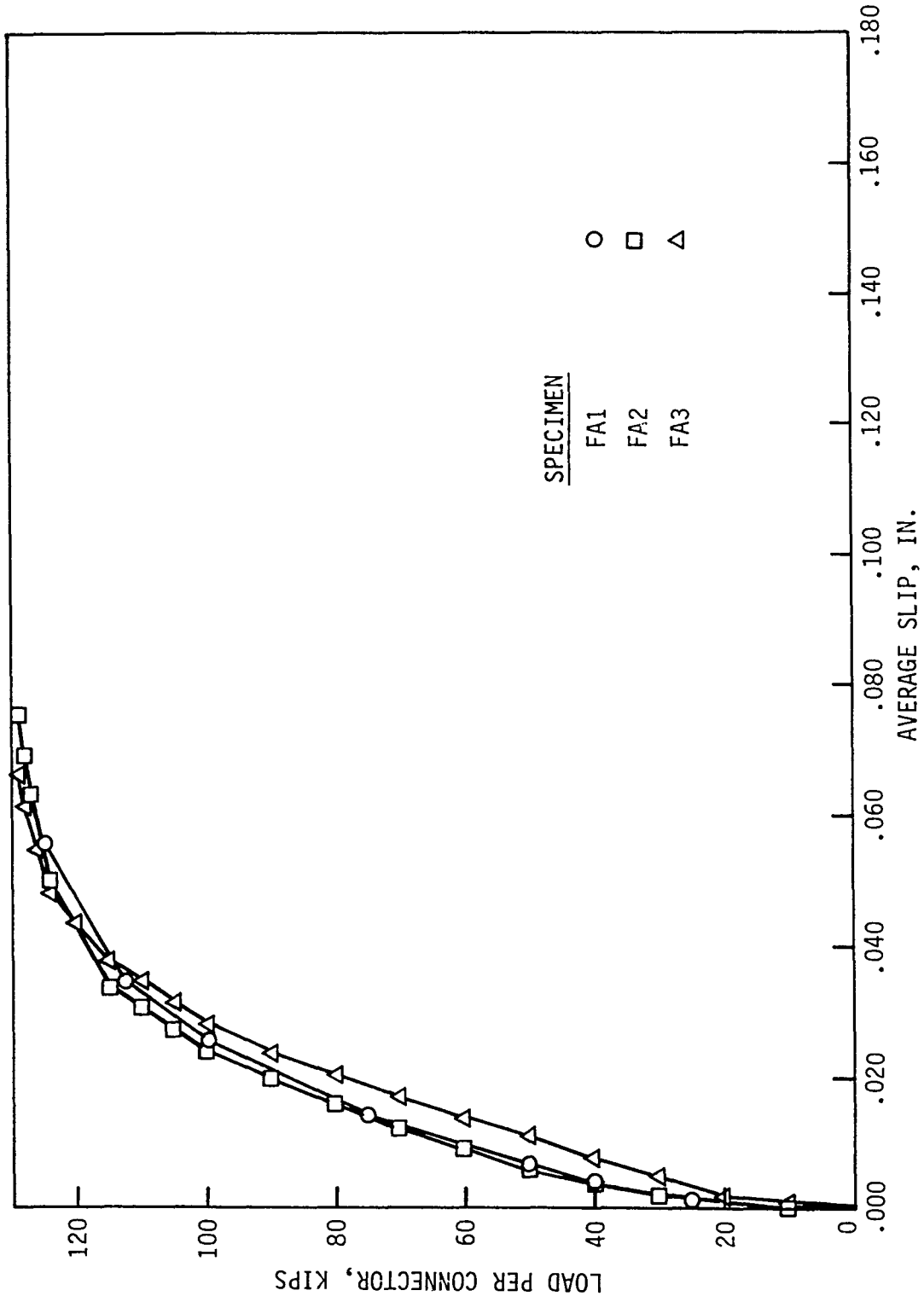


Fig. A.3. Load-slip curves for individual Series 3 push-out specimens

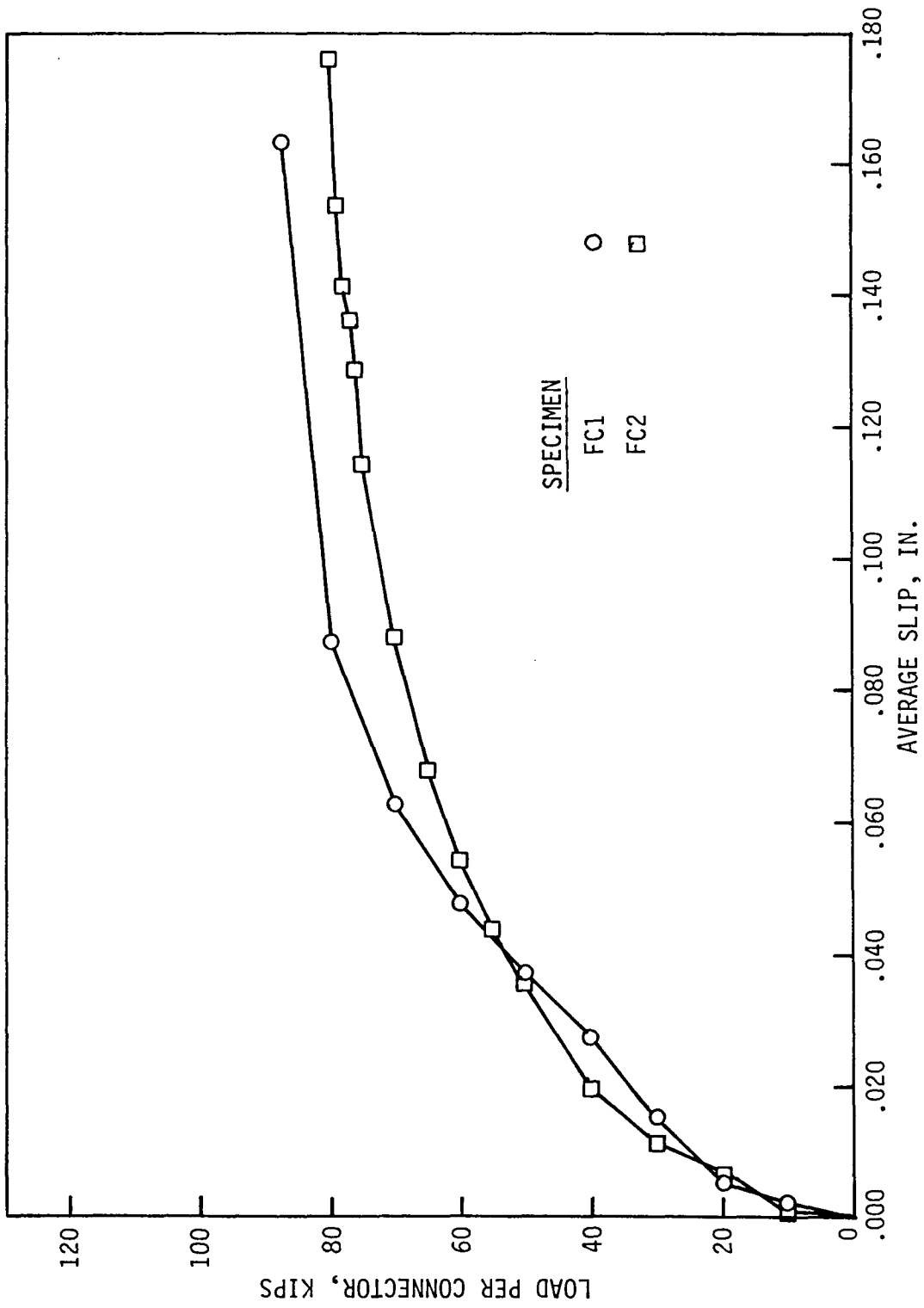


Fig. A.4. Load-slip curves for individual Series 4 push-out specimens

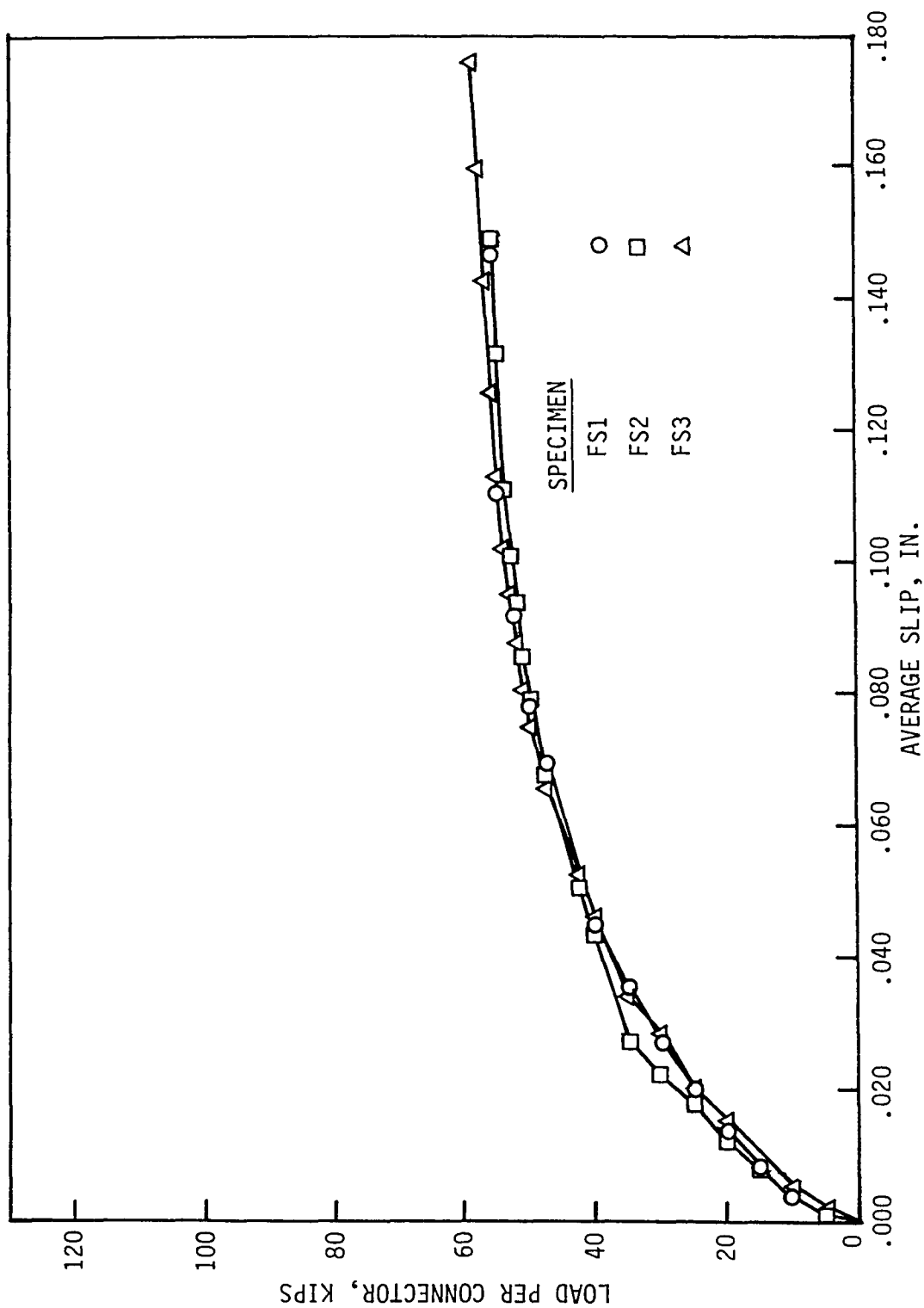


Fig. A.5. Load-slip curves for individual Series 5 push-out specimens

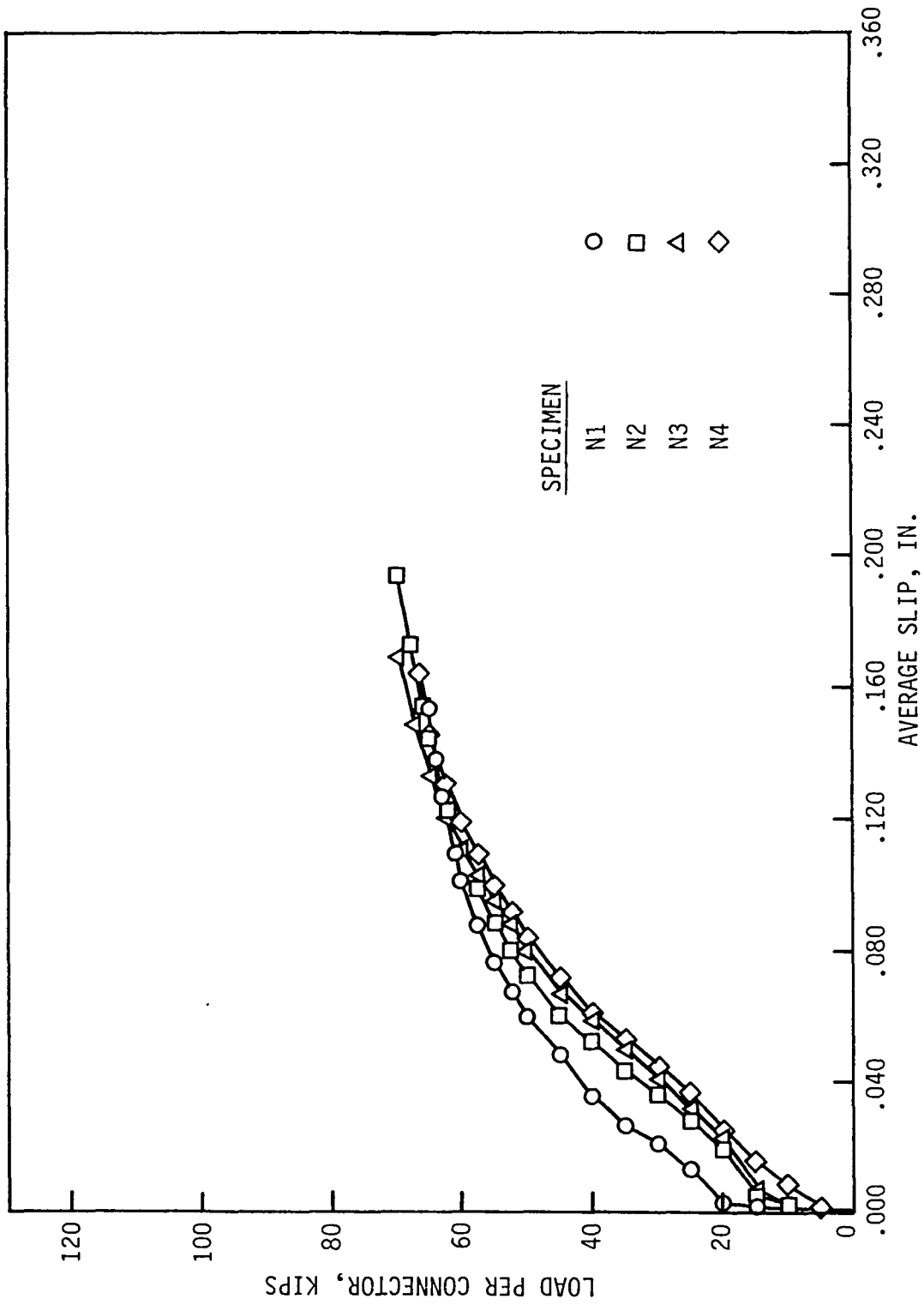


Fig. A.6. Load-slip curves for individual Series 6 push-out specimens

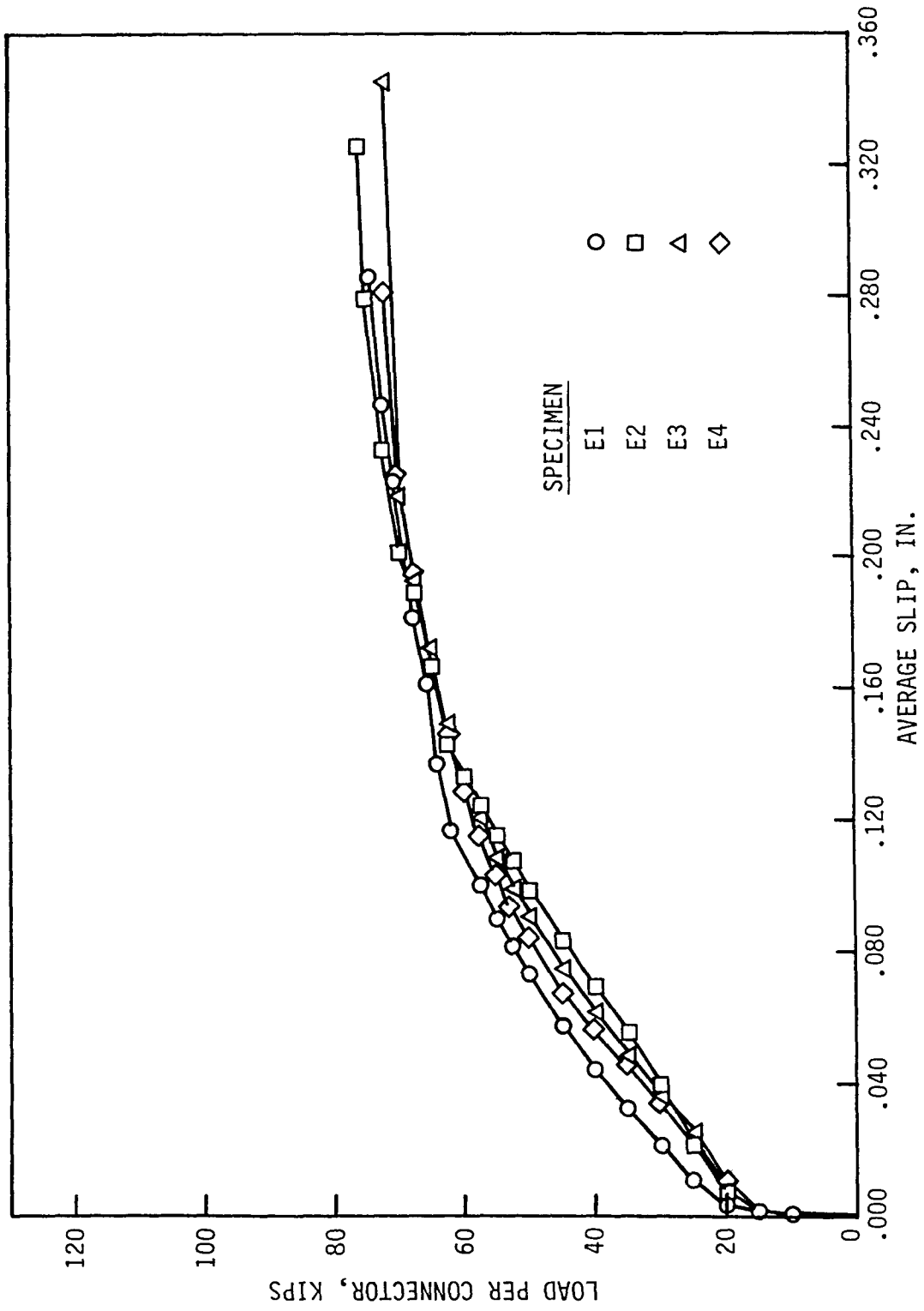


Fig. A.7. Load-slip curves for individual Series 7 push-out specimens

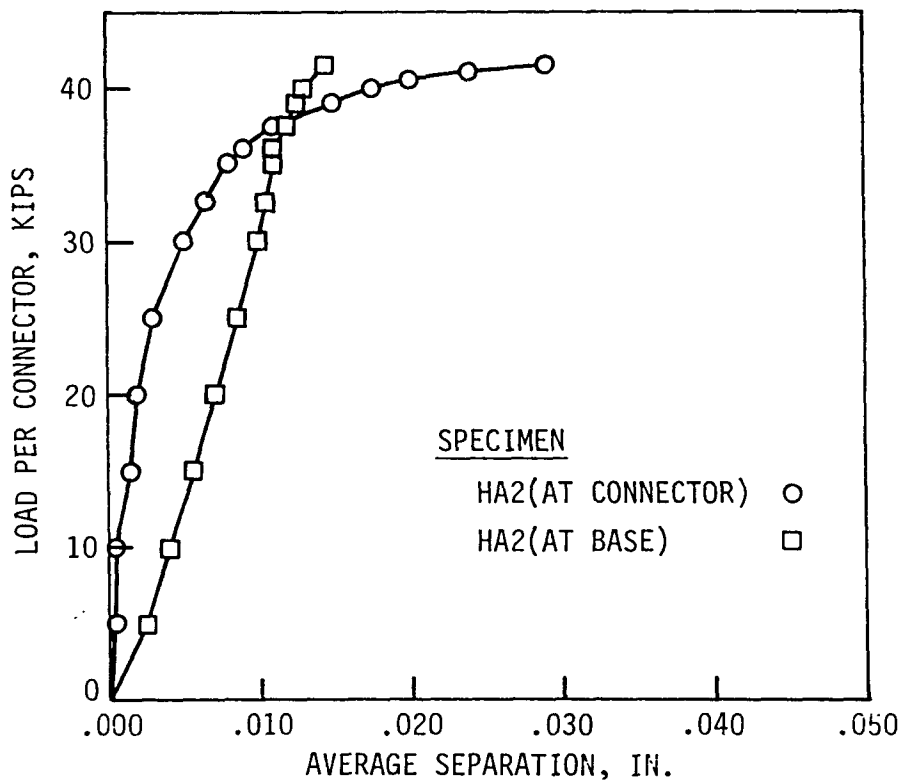


Fig. A.8. Representative load-separation curves for Series 1 push-out specimens

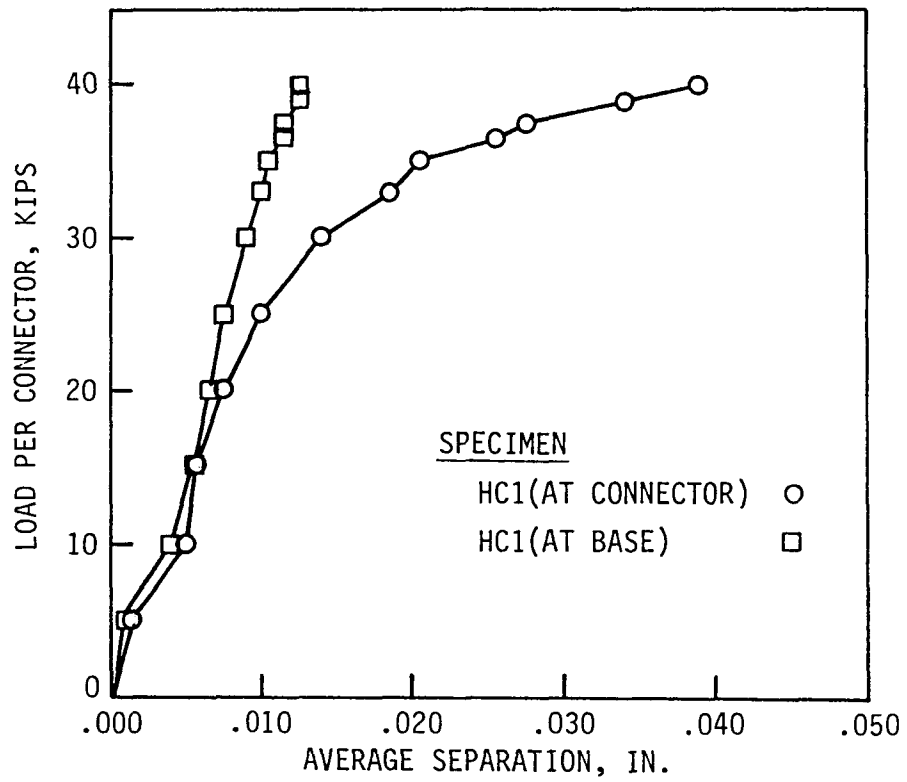


Fig. A.9. Representative load-separation curves for Series 2 push-out specimens

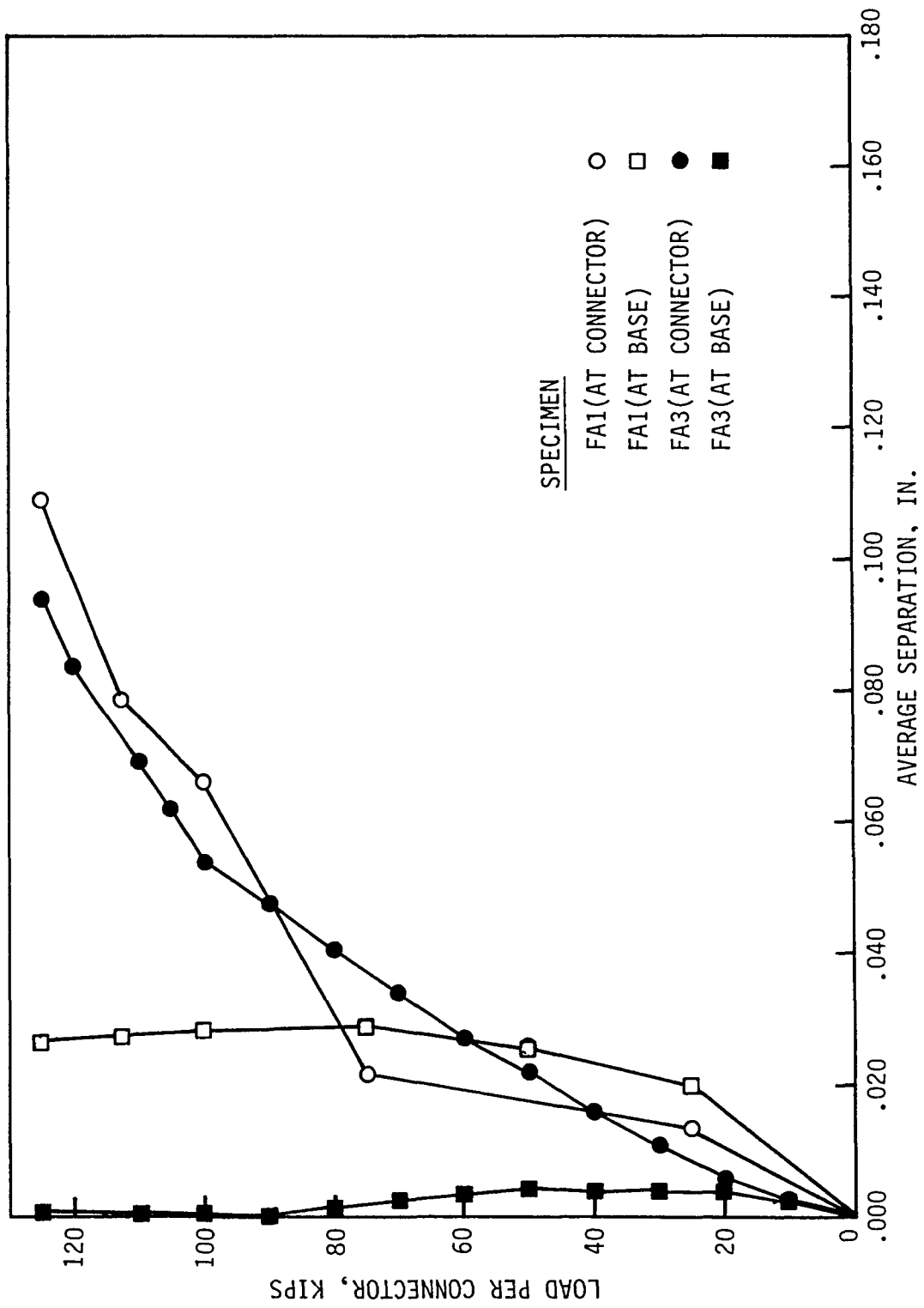


Fig. A.10. Representative load-separation curves for Series 3 push-out specimens

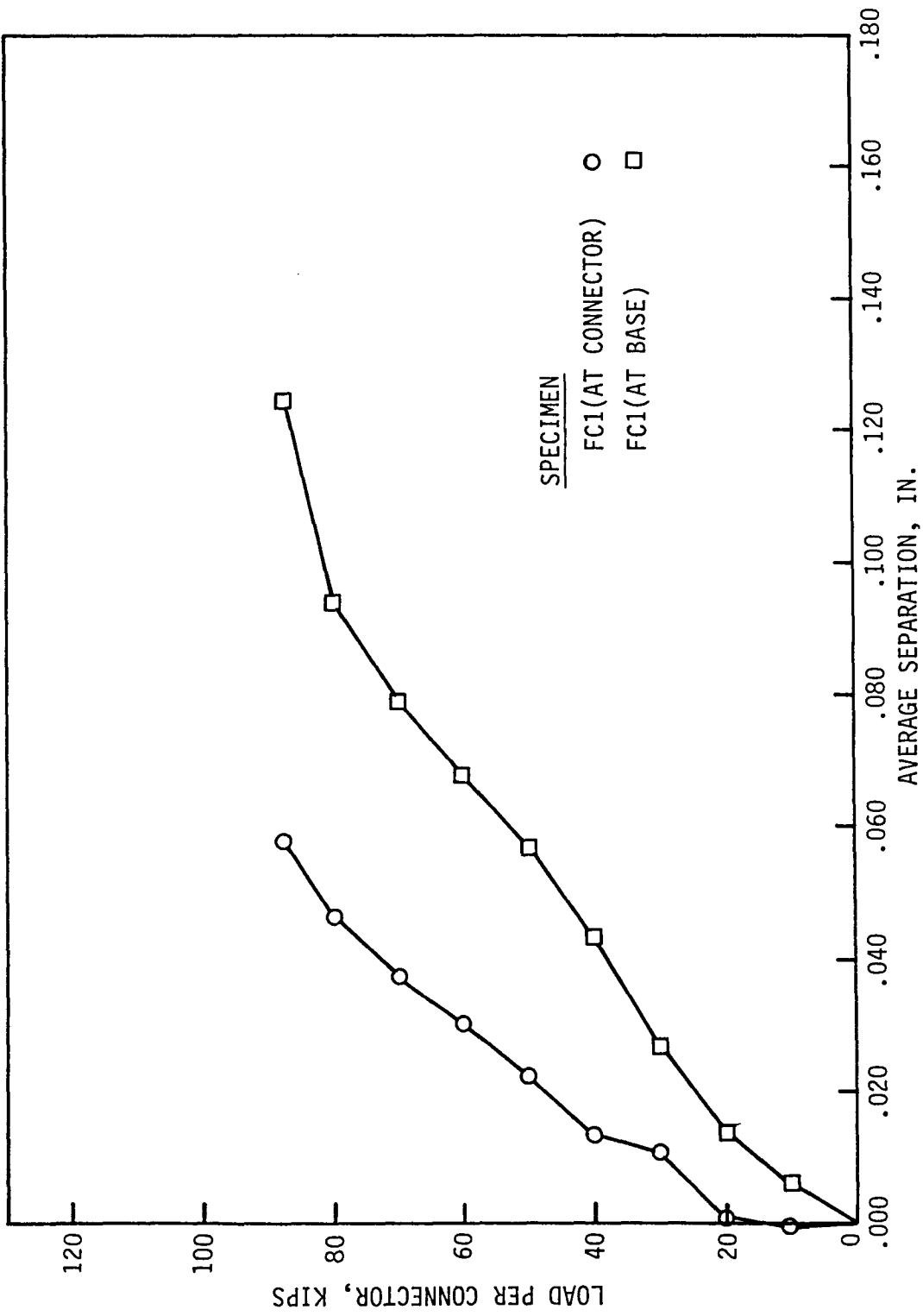


Fig. A.11. Representative load-separation curves for Series 4 push-out specimens

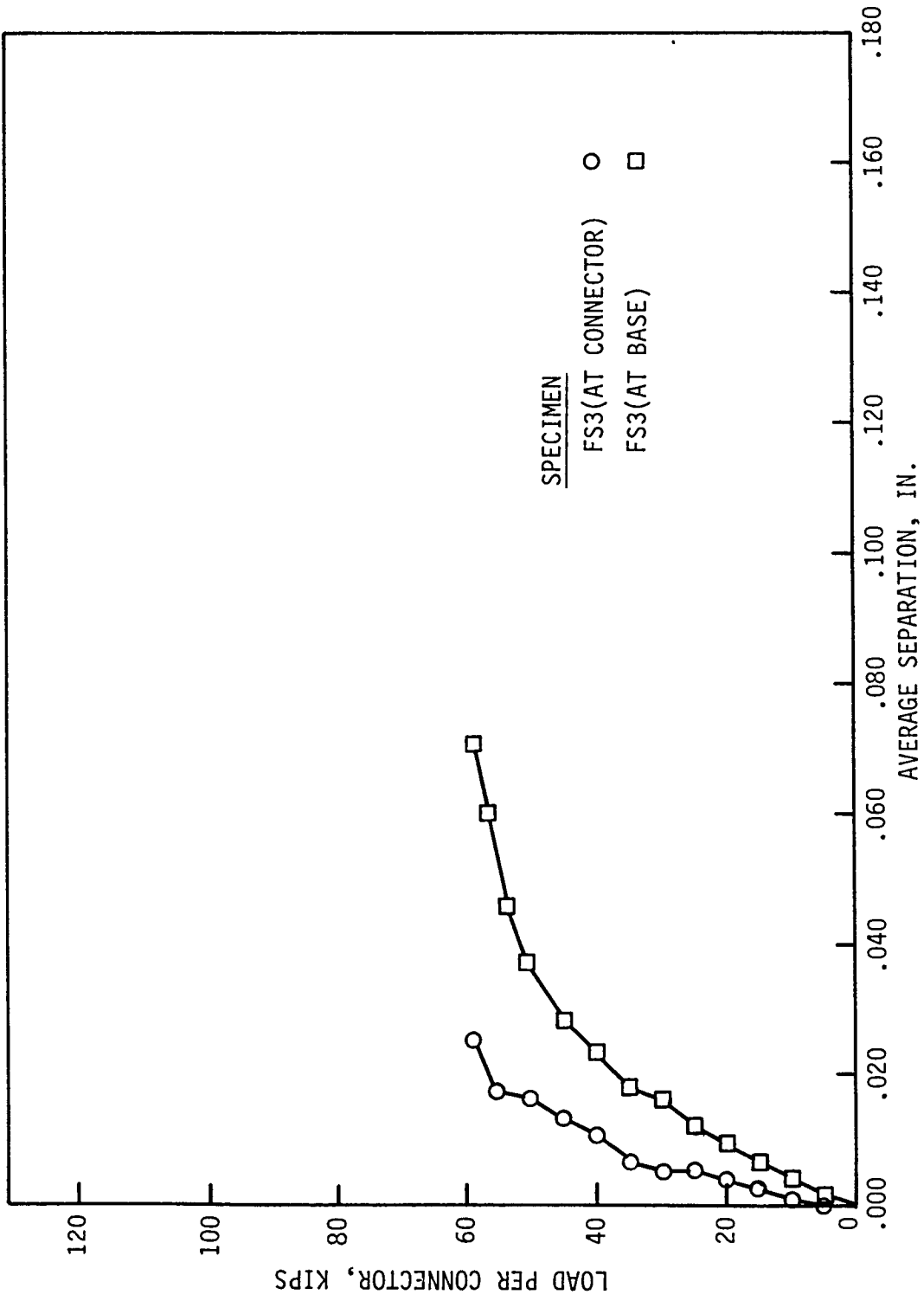


Fig. A.12. Representative load-separation curves for Series 5 push-out specimens

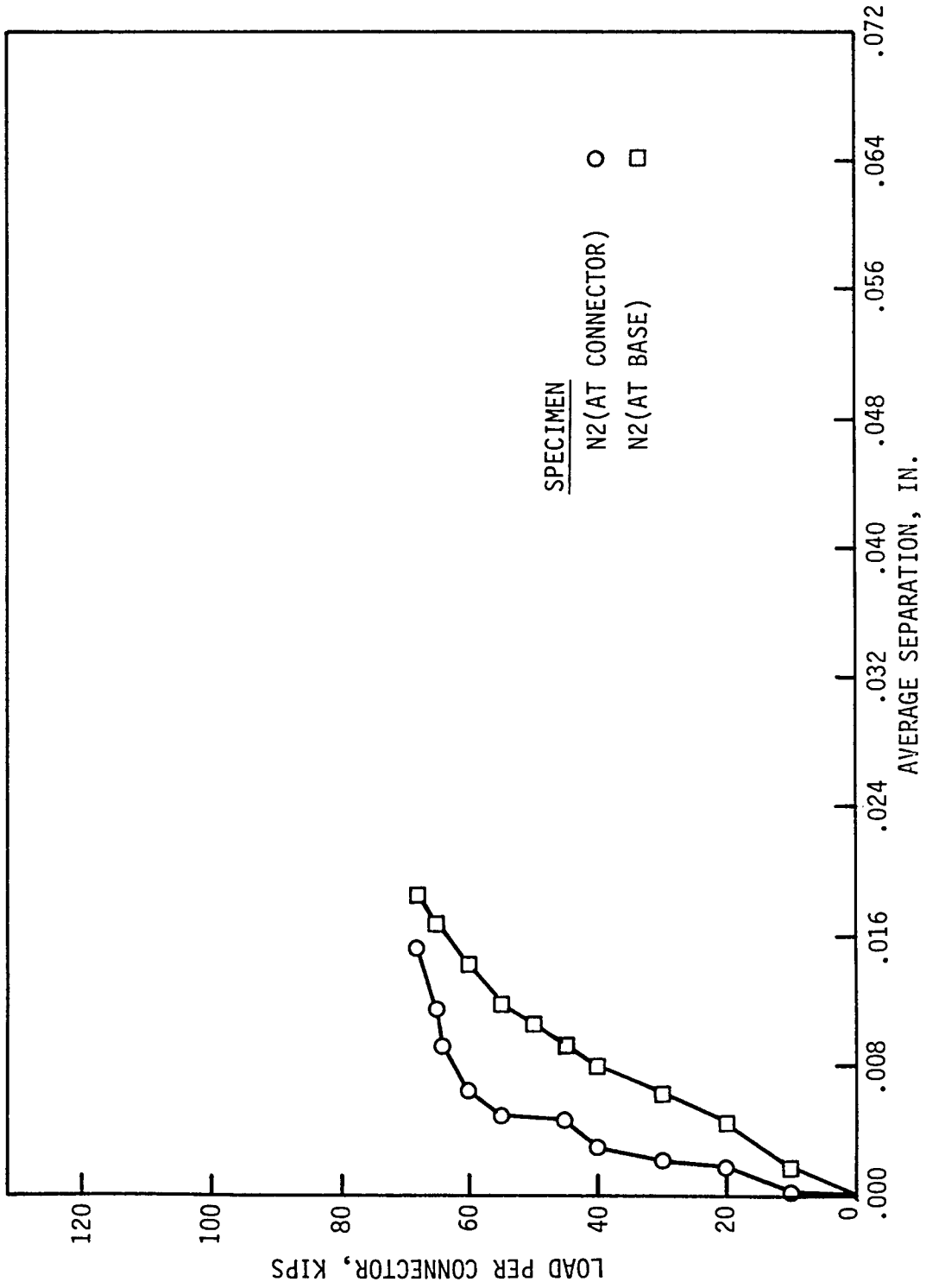


Fig. A.13. Representative load-separation curves for Series 6 push-out specimens

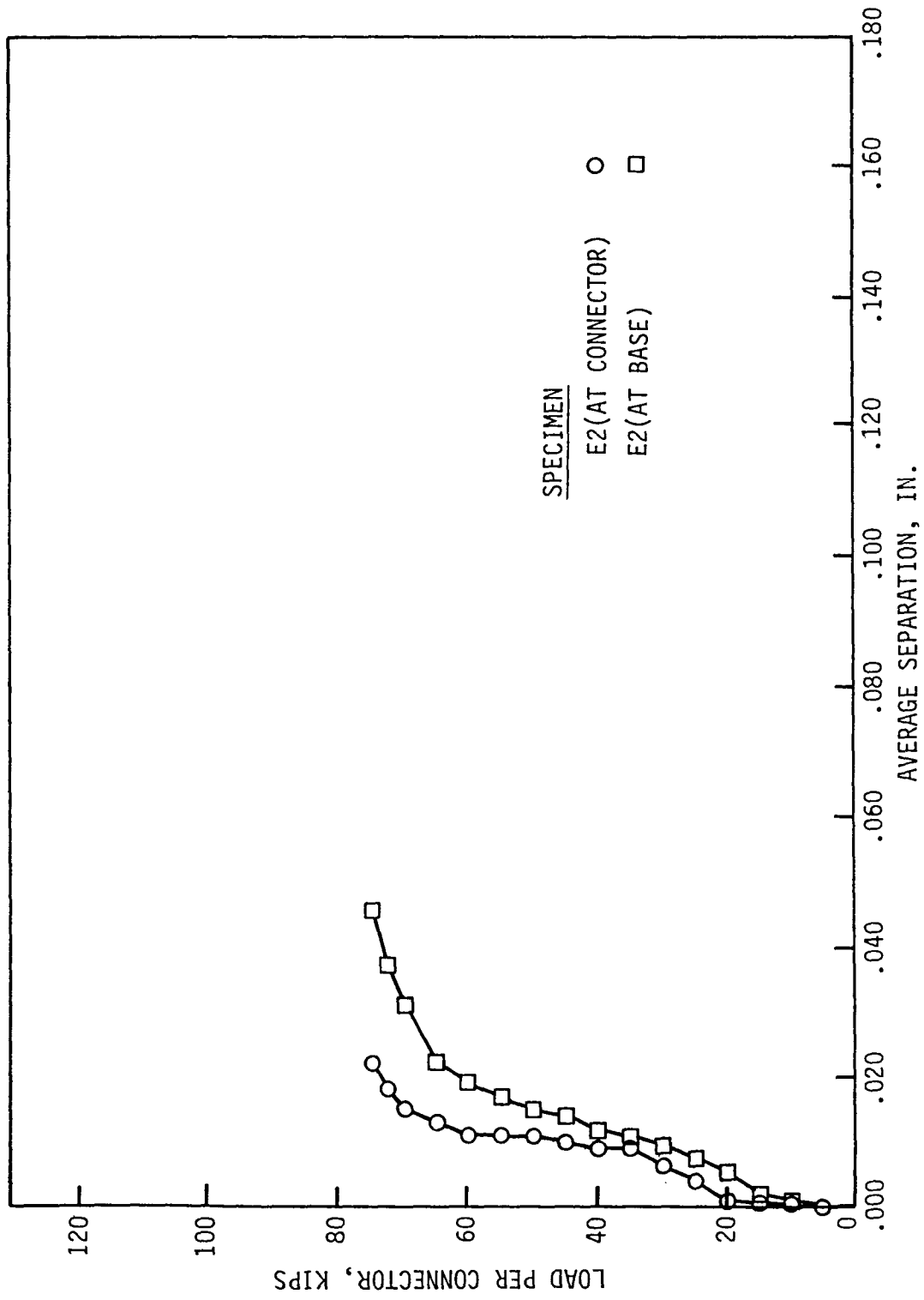


Fig. A.14. Representative load-separation curves for Series 7 push-out specimens